GEAP-10170
AEC RESEARCH AND
DEVELOPMENT REPORT
MARCH 1970

THE EFFECT OF STRESS CONCENTRATION ON THE LOW-CYCLE FATIGUE OF THREE LOW-STRENGTH STRUCTURAL STEELS AT ROOM TEMPERATURE AND 550°F

E. KREMPL

U. S. ATOMIC ENERGY COMMISSION
CONTRACT AT(04-3)-189
PROJECT AGREEMENT 37

GENERAL ELECTRIC

DISCLAIMER

GEAP-10170
AEC Research and
Development Report
March 1970

THE EFFECT OF STRESS CONCENTRATION ON THE LOW-CYCLE FATIGUE OF THREE LOW-STRENGTH STRUCTURAL STEELS AT ROOM TEMPERATURE AND 550°F

E. Krempl

Approved: S. R. Vandenberg
Project Engineer

Approved: D. H. Imhoff, Manager
Development Engineering

Prepared for the
U. S. Atomic Energy Commission
Under Contract Number AT(04-3)-189
Project Agreement 37

Printed in U.S.A. Available from the
Clearing House for Federal Scientific and Technical Information
National Bureau of Standards, U.S. Department of Commerce
Springfield, Virginia
Price: $3.00 per copy

ATOMIC POWER EQUIPMENT DEPARTMENT ● GENERAL ELECTRIC COMPANY
SAN JOSE, CALIFORNIA 95125

GENERAL ELECTRIC

6088—Dev.Eng.—48
250—MS—9/70

LEGAL NOTICE

This report was prepared as an account of Government sponsored work. Neither the United States, nor the Commission, nor any person acting on behalf of the Commission:

A. Makes any warranty or representation, expressed or implied, with respect to the accuracy, completeness, or usefulness of the information contained in this report, or that the use of any information, apparatus, method, or process disclosed in this report may not infringe privately owned rights; or

B. Assumes any liabilities with respect to the use of, or for damages resulting from the use of any information, apparatus, method, or process disclosed in this report.

As used in the above, "person acting on behalf of the Commission" includes any employee or contractor of the Commission, or employee of such contractor, to the extent that such employee or contractor of the Commission, or employee of such contractor prepares, disseminates, or provides access to, any information pursuant to his employment or contract with the Commission, or his employment with such contractor.

TABLE OF CONTENTS

LIST OF TABLES

LIST OF ILLUSTRATIONS

List of Illustrations (Continued)

ABSTRACT

The results of a 4-year testing program on the notched high-strain fatigue behavior of three low-strength structural steels are summarized. The parameters studied were: type of loading, push-pull and bending; influence of mean stress, completely reversed and zero-to-tension loading; state-of-stress, flat plates and grooved cylinders; degree of stress concentration, $K_t = 1.3$ to $K_t = 3.3$; and temperature, room temperature and 550°F. Notch-root strains were measured and fatigue strength reduction factors are derived. A reasonably conservative life calculation procedure for low-cycle fatigue crack initiation in the presence of stress concentration is proposed and recommended for consideration in design.*

1. INTRODUCTION

The crack initiation behavior under cyclic loading in notched structural members made out of three low-strength structural steels (carbon steel, 2-1/4 Cr—1 Mo alloy steel, and Type 304 stainless steel) was studied at stress levels leading to relatively short crack initiation lives. The influence of such parameters as notch sharpness, state-of-stress (flat plates, grooved cylinders), type of loading (completely reversed, zero-to-tension), stress gradient (bending, push-pull), and temperature were investigated. Table 1 shows the parameters that were studied during the program.

Raw data of the tests were reported in quarterly progress reports. After the completion of certain subtasks, topical reports were issued to interpret and analyze the data. Table 2 lists all reports issued and the subjects covered.

The purpose of this final report is to correlate and analyze the data, to interpret them, and to recommend a design application based on the results of this study.

From the beginning of this program, the stress (strain) concentration factor was distinguished from the fatigue strength reduction factor. The former characterizes the magnitude of the local stresses and strains in the root of the notch but does not give any information on the damaging effect of these strains or stresses. To characterize the fatigue damage done to a notched structural member, fatigue tests must be run so that the fatigue strength reduction factor can be determined. A comparison of the fatigue strength reduction factors with the stress (strain) concentration factor obtained under relevant conditions can then be used to ascertain whether the stress (strain) concentration factor may be used as a substitute for the fatigue strength factor. Consequently, the program was directed to obtain fatigue strength reduction factors for the various parameters listed in Table 1.

2. TEST CONDITIONS AND MATERIALS

During the tests, the variation of the notch-root strain range with cycling was measured on a number of specimens, using electrical foil strain gages with a minimum grid size of 1/64 inch. Crack initiation was monitored by a 20X microscope and red dye penetrant techniques. Crack initiation was said to have occurred when a crack of 0.005 to 0.015 inch was detected in the root of the notch. For the smooth-bar tests, crack initiation was determined as the drop-off point in the record of load range versus cycles. All tests on notched specimens were run under load control and at a frequency of about 6 cpm. Smooth-bar tests were conducted at the same frequency; however, strain control and completely reversed conditions were used exclusively in this case.

The basic geometries of the two types of notched specimens are shown in Figures 1 and 2 (all figures are contained in Section 7). To achieve the various stress concentration factors listed in Table 1, it was necessary to vary the minimum diameter of the bar and the notch-root radius. The bend tests were performed on doubly notched rectangular bars of 3 X 3 inch unnotched cross section. Load control was used in conducting the cantilever-type tests. Details will be discussed later.

*Conducted by the author at the Materials & Processes Laboratory of the General Electric Company at Schenectady, N.Y. Dr. Krempl has since joined the faculty of Rensselaer Polytechnic Institute at Troy, N.Y.

The mechanical properties at 550°F and room temperature and the chemical composition of the three materials are shown in Tables 3 and 4, respectively. All materials were tested in the annealed condition.

3. TEST RESULTS

In the discussion of the test results, average curves drawn through the experimental data points will be used for the calculations rather than individual test data. No scatter of the test results can be shown because of this method. Also, the limited number of tests does not permit a reliable estimate of the scatter of the data. All the data should therefore be considered as an indication of the trend of the real statistical relationship between applied load and life-to-crack initiation.

3.1 INITIAL NOTCH-ROOT STRAIN

The measurement of the cyclic elastic and plastic strains in the root of the notch enabled the construction of nominal stress range (always based on the net section area) versus notch-root strain range diagrams. For the different K_t values tested, these diagrams should reveal a family of nonintersecting curves. The curves for the three materials are shown in Figures 3 through 5 and apply for the grooved cylinders under completely reversed load-controlled loading. The strain ranges are measured at the beginning of the cycling test. The nominal stress notch-root strain behavior of zero-to-tension controlled specimens (which exhibited almost completely elastic action after the first cycle) is shown in Figure 2 of Reference 1. The transverse strain range curves are not shown in Figures 3 through 5. In previous reports, it was shown that the transverse strain range was at least a factor of 10 smaller than the axial notch-root strain range.

An inspection of Figures 3 through 5 reveals that the family of nonintersecting curves is obtained with only one exception (see Figure 4).

The cyclic stress-strain diagram (K_t, = 1.0) of Type 304 stainless steel intersects the curve for K_t = 1.9. In the smooth-bar cyclic tests, the stainless steel showed initial strain hardening followed by strain softening (GEAP-5082, Figures 6 through 8) for strain ranges below 1.2 percent. The cyclic stress-strain diagram was determined at $N_f/2$.* At this point, the stress range was less than the initial value. If the initial maximum stress range is used instead of the stress range at $N_f/2$, another stress-strain diagram is obtained (see Figure 4). This initial cyclic stress-strain diagram does not intersect the other curves.

For a good comparison and analysis, it is therefore necessary to recognize that there are property changes due to cyclic plastic straining and that every comparison should be based on the same cyclic age (which denotes the status of cyclic hardening or softening of a particular material). Figure 4 shows that discrepancies may result if the comparison is made at different cyclic ages of two sets of data.

Carbon steel and 2-1/4 Cr–1 Mo alloy steel showed cyclic strain hardening. The curves for the notched bars were always below the cyclic stress-strain curve. The notch-root strains were taken during the initial step-up tests (see Reference 2) for the procedure. Then, cyclic hardening caused the notch-root strain range to decrease (see Figure 6). The decrease was more pronounced at the high notch-root strain ranges than at the low ones. No indication of a cyclic steady-state was obtained because the strain gages failed while the notch-root strain range was still decreasing. If the curves for the notched specimens had been constructed for a postulated shake-down condition, they would have been much closer (lower strain range at the same nominal stress range) to the smooth-bar curves.

Comparisons of the type shown in Figures 3 and 5 are, therefore, easy for strain-hardening materials. Problems may arise for cyclic strain softening materials, as shown by the results for Type 304 (Figure 4).

It is not known how a multiaxial state-of-stress influences the cyclic hardening or softening behavior of a material nor whether a shake-down condition exists. This type of research is needed because it will ultimately improve the reliability of structural components.

*(N_f is the number of cycles-to-crack initiation.)

Another possibility would be to plot the monotonic stress-strain values on the stress-range versus strain-range curves shown in Figures 3 through 5. It was found that these curves intersected all notched specimen curves. Therefore, no good correlation was obtained between the monotonic stress-strain diagram and the nominal stress notch-root strain diagrams for notched specimens.

3.2 STRESS RANGE VERSUS CRACK INITIATION

The load range was kept constant during each notched specimen test. For each parameter, three to six specimens were tested at different stress levels and crack initiation was observed. At a given stress range, the severity of the stress concentration effect should be exhibited by appropriately displaced crack initiation curves. This is shown by the crack initiation data plotted in Figures 7 through 9, using the applied nominal stress ranges. Curves of the shake-down stress range versus cyclic life for the strain-controlled smooth-bar tests are also shown. The crack initiation points plot on straight lines, which are not always parallel to each other. The steady-state stress ranges of the smooth-bar data show the longest lives (as should be expected).

A check was made as to whether errors in experiments or in data reporting were responsible for the anomalous behavior of the $K_t = 1.9$ data for the 2-1/4 Cr–1 Mo material in Figure 9. No error could be found and no reason for the steep slope of this test series can be given.

The influence of mean stress on the deformation and fracture behavior was discussed extensively in Reference 1 for $K_t = 3$ specimen series. The influence of the parameter temperature (550°F) was investigated separately in Reference 3. Although the influence of these two parameters was investigated and discussed for $K_t = 3$ only, it is not unreasonable to assume that the same trend of the data will be observed for stress concentration factors different from $K_t = 3$. Therefore, the influence of temperature and mean stress will not be considered here.

3.3 ANALYSIS OF NOTCHED BEND TESTS

Bend tests were performed to assess a possible influence of the gradient of the stress field on crack initiation. The bend test specimen is shown in Figure 10. The tests were load-controlled, and a cantilever type of load application was used (see Reference 4). The stress concentration factor was determined to be about $K_t = 1.8$ (uniaxial and plane stress condition, which is only approximately met by the test bars). Only two test materials were used in this case–2-1/4 Cr–1 Mo alloy steel and Type 304 stainless steel.

A comparison of push-pull with bend tests on a stress basis is difficult if the nominal stresses are beyond the elastic range. The conventionally calculated stress in a bend test is based on elastic material behavior. For the push-pull test, the nominal stress can be obtained directly. For a good comparison, an elasto-plastic analysis must be performed for the bend tests. The approximate elasto-plastic analysis used in this report will be described in the following equations.

In conventional engineering analysis methods, the nominal bending stress is obtained by:

$$\sigma = \frac{Mc}{I} \tag{1}$$

where M = amplitude of applied moment,
c = maximum distance from neutral fiber, and
I = area moment of inertia.

The stress ranges calculated in this way are plotted in Figures 11 and 12, with push-pull data for $K_t = 1.9$ and $K_t = 3.3$. The bending stress ranges plot high on each of the figures, and the large difference between the bending and push-pull results can be observed.

Equation (1) assumes elastic material behavior which is not valid for the tests discussed here. Therefore, a simplified elasto-plastic analysis must be used for calculation of the nominal stress range. To accomplish this, the cyclic stress-strain diagram of each material will be used. The cyclic stress-strain diagram can be idealized in the following way:

Type 304 Stainless Steel

$$\sigma = E\epsilon \qquad \text{for } o \leqslant \epsilon \leqslant \epsilon_o \tag{2}$$

$$\sigma = \sigma_o + (\epsilon - \epsilon_o)\, E_{II} \text{ for } \epsilon > \epsilon_o \,.$$

2-1/4 Cr–1 Mo Steel

$$\sigma = E\epsilon \qquad \text{for } o \leqslant \epsilon \leqslant \epsilon_o \tag{3}$$

$$\sigma = \sigma_o + A(\epsilon - \epsilon_o)^{II} \quad \epsilon > \epsilon_o.$$

The symbols denote:

σ,ϵ	=	stress and strain, respectively,
σ_o,ϵ_o	=	stress and strain value, respectively, at which the stress-strain curve departs from linearity,
E	=	modulus of elasticity,
E_{II}	=	slope of second section of the bilinear cyclic stress-strain curve of stainless steel,
A	=	constant, dimension of stress,
n	=	strain hardening exponent.

The constants must be determined so that the equations reproduce the cyclic stress-strain diagram (see Reference 5).

Equilibrium requires that the moment of the stresses balances the external moment (M). Thus, we have

$$M/2 = \int_o^h \sigma z dz, \tag{4}$$

where h = distance from neutral axis to notch-root, and
z = coordinate perpendicular to neutral axis (see Figure 10)

For the two sections of the stress-strain diagram we get

$$M/2 = \int_o^{z^*} E\epsilon z dz + \int_{z^*}^h (\sigma_o + (\epsilon - \epsilon_o)\, E_{II}) z dz \tag{5a}$$

for stainless steel; and

$$M/2 = \int_o^{z^*} E\epsilon z dz + \int_{z^*}^h [\sigma_o + A(\epsilon - \epsilon_o)^n]\, z dz \tag{5b}$$

for 2-1/4 Cr–1 Mo alloy steel.

---

z* denotes the distance from the neutral fiber at which the stress distribution departs from linearity. It can be obtained from Equation (1) by solving for c = z* and substituting σ_o for σ.

The assumption is made that plane sections remain plane.

$$\epsilon = \kappa z, \tag{6}$$

where κ is the constant curvature of the beam. Equation (6) is substituted into Equations (5a) and (5b). These equations can be solved for κ, which, in the case of Equation (5b), must be done by trial and error. Once κ is determined, the nominal maximum strain can be derived from Equation (6). The second of Equations (2) or (3) determines then the maximum nominal stress σ_N cyclic. This value is for a bend bar without notches having a width equivalent to the minimum width of the actual test bar shown in Figure 10.

The thus calculated values of the stress amplitudes σ_N cyclic are, of course, lower than the ones derived from Equation (1). The values of σ_N cyclic are given in Table 5 with other pertinent data of the bend tests. The new results of the bend tests are then plotted in Figures 11 and 12. It can be seen that the correlation with the push-pull data is much better using the stress range values based on the cyclic stress-strain diagram.

Figure 11 shows that the results of the tests with stainless steel and the bending results ($K_t = 1.8$) fall somewhat below the results for $K_t = 1.9$, which constitutes a reversal of the expected order. Therefore, it can be said that the introduction of the nominal stress based on the cyclic stress-strain diagram improved the correlation with push-pull tests, but not quite the way it should have.

The situation is far better for 2-1/4 Cr—1 Mo alloy steel (Figure 12). The correlation between push-pull and bend tests is good on the basis of the σ_N cyclic. The point at the low stress range plots on the wrong side of the $K_t = 1.9$ curve for push-pull. The crack was 1/4 inch in size when it was detected during this test. Actually, crack initiation had occurred earlier than the cyclic life plotted, as indicated by the arrow.

The elasto-plastic analysis of the bend tests greatly improved the correlation with the push-pull tests. However, an exact one-to-one correlation was not achieved.

From the analysis, it can be seen that the desired statement on the possible influence of the stress gradient cannot be made with confidence. The 2-1/4 Cr—1 Mo data do not indicate such an influence on the results; however, the tests with Type 304 stainless steel suggest that a life reducing influence of the gradient may exist. However, it is felt that the test results are too limited to make such a definite statement. Until further evidence is available, it is assumed that the stress concentration factor *per se* is the prime parameter to describe the notch effect in low-cycle fatigue for bending and push-pull.

3.4 NOTCH-ROOT STRAIN RANGE VERSUS CRACK INITIATION

Frequently, the statement is made that the strain range (or plastic strain range) is the prime criterion for low-cycle fatigue. This implies that the knowledge of the strain range (or plastic strain range) at a critical location would enable the prediction of the fatigue life of the component, provided the basic smooth-bar fatigue curve of the same material were available.

The notch-root strain measurements provide an opportunity to check on this hypothesis for the total strain range. It is not possible to directly extract the real plastic strain range from the load notch-root strain range hysteresis loops. It is not known at what value of the nominal stress the stress in the apex of the notch reaches zero; therefore, the local plastic strain cannot be determined without additional assumptions.

However, one other complicating factor arises in a comparison on the basis of strain range. In a smooth-bar test, the strain range is kept constant, whereas a possibility exists for the strain range in the root of the notch to change during cycling (see Figure 6). The materials investigated in this study were all cyclic strain hardening (with the exception of stainless steel), so that the strain range in the root of the notch decreased (as shown in Figure 6) or stayed constant at lower nominal stresses. To make a fair comparison, the strain ranges should be compared at the same cyclic age of the material. In light of the limited

information on the variation of the notch-root strain with cycles and the absence of any information of the influence of the stress state on cyclic hardening, it was thought best to compare the initial strain ranges. The results of the comparison are shown in Figures 13 through 15. Compared with the nominal stress range plots in Figures 7 through 9, the spread between the data in Figures 13 through 15 is considerably reduced. However, a perfect correlation was not achieved on the basis of the strain range data. It might be argued that the different definitions of crack initiation in the smooth-bar and notched-bar tests could be responsible for the spread. However, some spread exists even within the set of notched data where the definition is consistent.

Of special interest are the data for the 2-1/4 Cr–1 Mo material, where it appears that $K_t = 1.9$ results in the shortest lives for a given strain range. Both the bars with $K_t = 3.3$ and $K_t = 1.3$ crack much later at the same strain range. The same trend is evident for Type 304 stainless steel in Figure 14. However, the carbon steel data in Figure 13 exhibit near uniform cracking strain ranges for both $K_t = 1.9$ and $K_t = 3.3$.

A good correlation is obtained between the bending and push-pull data when the correlation is based on strain range. Finally, it is fair to say that the notch-root strain range versus cycles-to-crack initiation plots showed a much better correlation than did the nominal stress range plots. A unique relationship for the strain ranges which would qualify them as unique fatigue indicators could not be found. The difficulties mentioned at the beginning of this section may be partly responsible for the lack of perfect agreement.

A correlation on the basis of an effective strain (maximum principal strain difference, von Mises) was attempted earlier for $K_t = 3.3$ (see Reference 6). The results showed no basic change in the correlation, such as a change of the slope of the fatigue life curves. The use of effective strains produced a parallel shift relative to the original curve: The assumption of deformation under constant volume must be made in calculating the effective strain. Therefore, this approach is not pursued further in this report.

3.5 FATIGUE STRENGTH REDUCTION FACTOR

In earlier reports, the need for a clear definition of the fatigue strength reduction factor in the low-cycle fatigue regime was pointed out repeatedly. It was stated that the different fatigue strength reduction factors obtained in various investigations are caused mainly by two factors: (1) the different definitions of the derived fatigue strength reduction factors, and (2) different definition of cycles-to-crack initiation (which is often actual failure of the test bars).

Within the conditions of this study (strain-controlled smooth-bar data, load-controlled notched-bar tests), three different definitions of the fatigue strength reduction factor are possible, as indicated in Figure 16 and described further in Reference 6. The Method IA and Method II factors were found to be always higher than the theoretical elastic stress concentration factor. The Method IA factor usually reaches a maximum, whereas a continuous increase is observed for the Method II factor. Both factors are identical if the nominal stress range of the notched specimen is in the linear range of the cyclic stress-strain diagram. The Method IB factor, however, was never larger than the theoretical elastic stress concentration factor and decreased with increasing stress amplitude.

4. ANALYSIS OF NOTCH-ROOT STRAIN

The ultimate decision as to what factor might be most useful in design applications must be based on a comparison of the derived fatigue strength reduction factors with analytically determined stress or strain concentration factors. Only the latter factors can presently be calculated from theoretical considerations. It would be most helpful if the factors derived in the analysis would provide an upper bound of the fatigue strength reduction factor. Such a situation exists in high-cycle fatigue where the theoretical elastic stress concentration factor is always higher than the fatigue strength reduction factor. Therefore, the theoretical elastic stress concentration factor, K_t, is often used in design instead of the actual fatigue strength reduction factor, on the basis that this leads to a conservative procedure.

Two approximate methods are available (developed by Stowell[7] and Neuber[8]) for determining the stress and strain concentration factors beyond the elastic range. In each case, stress and strain concentration factors can be derived for any nonlinear stress-strain law.

A computer program* using the Stowell method was developed earlier at Schenectady General Electric. Therefore, this method was used in the following paragraphs.

4.1 STRESS AND STRAIN CONCENTRATION FACTORS

The stress-strain diagram used in the calculations was the cyclic stress-strain diagram of each material. With the computer program and the cyclic stress-strain diagram, stress and strain concentration factors were obtained for each K_t value listed in Table 1. The so-derived stress and strain concentration factors were then compared to the experimentally obtained fatigue strength reduction factors. It was found that the Method IB factor corresponded closely to the stress concentration factor. The Method IA factor showed a variation with applied stress amplitude similar to the strain concentration factor.

The results are shown in Figures 17 and 18 for 2-1/4 Cr—1 Mo alloy steel and in Figures 19 and 20 for carbon steel. The corresponding fatigue strength reduction factors are shown in each figure.

Problems developed in the calculation of the plastic stress and strain concentration factor for the Type 304 stainless steel. The bilinear, cyclic stress-strain diagram of this material is not suitable for the iterations necessary in the application of the Stowell method. For example, the calculated stress concentration factor showed an initial decrease followed by an increase with applied nominal stress amplitude. This trend of the variation is, of course, contrary to the physical evidence. The stress concentration factor decreases continuously with applied stress. A detailed study of the Stowell method and/or the computer program employed in the calculations would therefore be necessary for the case of a bilinear stress-strain diagram. Such a study was beyond the scope of this subtask. The discussion will therefore be limited to the carbon steel and the 2-1/4 Cr—1 Mo alloy steel results.

4.2 COMPARISON WITH FATIGUE STRENGTH REDUCTION FACTORS

Figures 17 and 19 indicate that there is a close correspondence between the Method IB fatigue strength reduction factor and the stress concentration factor.

The correspondence between the Method IA factor and the strain concentration factor shown in Figures 18 and 20 appears to be inferior to the one shown in Figures 17 and 19. Before a final judgment is made, it must be considered that Figures 17, 19 and 18, 20 express the same fact in different quantities, viz. stress and strain. It is therefore obvious that the difference is due to the way the relationship has been expressed. Strain is more sensitive than stress.

Because the Method II factor (Figure 16) is always higher or equal to the Method IA factor, the difference between the strain concentration factor and the Method II factor is equal or greater than the difference between the Method IA factor and the strain concentration factor.

It was mentioned earlier that the use in design of an analytically derived concentration factor instead of the actual fatigue strength reduction factor must be based on a comparison between the two factors. An analytically derived factor is very useful if it is always higher than the actual fatigue strength reduction factor. It appears that this requirement cannot always be met by the factors derived from the Stowell method. They are sometimes less than the corresponding fatigue strength reduction factors. The ultimate decision on the usefulness must be evaluated from an application of the analytically derived factors for life prediction and a comparison of the predicted life with the observed life. This comparison is made in the last section of this report.

*The author is indebted to Messrs. D. L. Newhouse and B. M. Wundt for permission to use the above-mentioned computer program.

4.3 NOMINAL STRESS RANGE–NOTCH-ROOT STRAIN RANGE

The Stowell method can also be used to calculate the nominal stress range versus notch-root strain diagrams for various stress concentration factors. The cyclic stress-strain diagram was again used in the calculations. Figures 21 and 22 compare the calculated and the measured nominal stress range notch-root strain range diagram for 2-1/4 Cr–1 Mo alloy steel and carbon steel, respectively.

For $K_t = 3.3$, the correlation is very good. For K_t values less than 3.3, the correlation leaves much to be desired.

At this point, it is worthwhile to list the approximations inherent in the method used. The present form of the Stowell method is an approximate calculation developed for plane stress. Any regular stress-strain diagram can be employed in the method.

The state-of-stress in the notched bars of this study is certainly not plane stress. The stress-strain diagram used refers to the cyclic steady state of the smooth-bar specimens. The strain range in the notch-root was not determined in the shake-down condition; rather, at the beginning of the test.

Therefore, two major approximations are involved in the comparison. The first one affects the state-of-stress in the specimen and, therefore, is geometrical in nature. The second one concerns the cyclic age of the material, which affects the stress-strain properties of the material and, therefore, is related to the material behavior (which should be characterized by its constitutive equation).

In cyclic plastic straining, metals show strain hardening or softening and the material changes its stress-strain properties from cycle to cycle. Ideally, one would therefore be interested in calculating the variation of the notch-root strain range from cycle to cycle. However, no constitutive equation is available which can reproduce cyclic strain hardening or softening (e.g., Reference 9). Thus, the cyclic stress-strain diagram is used as the best possible approximation.

Since the strains measured in the notch of the cylindrical bars are recorded initially, after the specimen had passed through step-up procedure (See Reference 2), they are at a different cyclic age compared to the steady-state stress-strain diagram. Indeed, the notch-root strain range continues to decrease for the cyclic strain hardening materials tested in this study (see Figure 6). At a later cyclic age, all the notch-root strain range curves will be displaced to smaller strain values and, therefore, the correlation with the measured values will improve.

It is not known how a multiaxial state-of-stress will influence the cyclic strain hardening or softening characteristics of materials. It may be that a multiaxial state-of-stress may increase or decrease the time necessary to reach the cyclic steady state. It is also conceivable that no cyclic steady state may be reached under certain conditions. Research involving stress analysis for cyclic plastic straining is definitely needed.

The main emphasis of this study was in the development of life calculation procedures. In these methods, a comparison is necessary between stress and strain concentration factors and the respective fatigue strength reduction factors. This can only be done if the method shows a reasonable degree of conservatism in life calculation. Since a conservative rather than an exact calculation is required, the degree of correlation shown in Figures 17 through 20 may be sufficient for our purposes. For the life calculation, an exact correlation of the strain data of the kind shown in Figures 21 and 22 is not required.

5. DESIGN APPLICATION

The information generated in this study can be used in the design components subjected to low-cycle fatigue loading in the presence of discontinuities.

The nominal (nonconcentrated) stresses are usually obtained by standard calculations or by finite element computer methods. Linear elastic material behavior is assumed in all these calculations, even if the local stresses or strains may be of such a magnitude that they will exceed the elastic limit of the material.

The objective of the life calculation, then, is to estimate the useful service of the component. At this point, it is necessary to combine the elastically calculated nominal stresses with the life information generated in this study or others. The cyclic plastic deformation is now recognized and the cyclic stress-strain diagram is generally used in the derivation of the factors relating to life. Therefore, approximations are involved in the life calculation, and one can only expect that the calculation will yield moderately conservative results. However, extreme conservatism in the calculation of the life is not desired, since it imposes too severe restrictions on the allowable stresses. Therefore, moderate conservatism is required for the approximate life calculation.

The results of the room temperature push-pull tests produced reasonable correlation between the calculated stress (strain) concentration factors and the corresponding fatigue strength reduction factors. Therefore, the factors derived from the Stowell method will be used to predict the life of the room temperature bend and the 550°F push-pull tests. For the life calculation, the following information is necessary:

a. For the notched member—nominal stress amplitude and uniaxial, elastic stress concentration factor.
b. Material properties—cyclic stress-strain diagram, variation of stress (strain) concentration factor with applied nominal stress (supplied by the Stowell method in this study), and smooth-bar low-cycle fatigue curve (completely reversed, strain control in this report).

The method will yield an estimate of the life-to-crack initiation (the appearance of a 0.005- to 0.015-inch-long crack), which can be compared with the experimentally observed crack initiation. Therefore, an independent check is obtained.

The general procedure is shown in Figure 23, which indicates that there are two equivalent methods—the stress approach and the strain approach. In theory, both will predict the same notch-root strain range and, therefore, the same life. In actual computation, great care must be exercised so that the theoretically expected outcome is obtained. Small errors in picking the values from the pertinent diagrams can be greatly amplified because of the nonlinear relations involved in the calculations.

Topper *et al.*,[10] developed a similar method based on Neuber's rule. In their study, no differentiation was made between initiation and final failure; also, mean stress, bending, and elevated temperatures were not considered.

5.1 LIFE PREDICTION OF THE 550°F PUSH-PULL TESTS

The smooth-bar fatigue life and the cyclic stress-strain diagram were determined for all three materials at 550°F (see Reference 3). The Stowell method and the cyclic stress-strain diagram were employed to calculate the stress and strain concentration factor as a function of the applied nominal stress amplitude for the theoretical elastic stress concentration factor of $K_t = 3.3$.

The strain range in the root of the notch corresponding to the cyclic steady state can then be calculated with either the stress or the strain concentration factor, as shown schematically in Figure 23. Both methods will yield the same result, in principle. However, it is possible that the notch-root strain range obtained by the strain or stress approach may differ somewhat because of inaccuracies in the procedure. Great care is therefore necessary in the calculation.

The notch-root strain range is then used to predict life-to-crack initiation. The comparison with the observed life is shown in Tables 6 and 7. As explained in the beginning of the report, observed values of cycles-to-crack initiation are taken from curves drawn through the initial data points.

Comparison of predicted and the observed life (taken from Figures 14 or 15 of Reference 3) shows that the prediction is somewhat unconservative for most of the points if the crack initiation data are considered. However, the prediction is very conservative if compared to the final failure of the notched bars. An estimate was made as to how deep the crack would have grown in the difference between the cycles observed and predicted, using the average crack growth rates given in Figure 17 of Reference 3. In no case of unconservative prediction would the crack have grown deeper than 0.065 inch. This degree of unconservative prediction appears to be acceptable, in light of the big safety margin with respect to the final failure of the grooved cylinders.

5.2 ROOM TEMPERATURE BEND TESTS

The previously used method can also be approximately applied to the case of life calculation in pure bending.

In the case of bending, the calculation can be based on the stress amplitudes calculated for either the elastic or the elasto-plastic material behavior. Both of these stress amplitudes were calculated previously (see Table 5).

The results of the life calculation (using the elasto-plastic material behavior and the method depicted in Figure 23) are shown in Table 8. It can be seen that the predictions are unconservative; i.e., larger than the observed values. If it is assumed that the crack grows with the same average crack growth rate in bending as in push-pull, it can be estimated (using data from Reference 1) that the crack could have grown a maximum 0.160 inch in depth in the cycle interval between actual crack initiation and the one predicted for the worst case. This amount of crack growth may be severely limiting.

In the case of bending and in any other case where the stresses are statically indeterminate, fictitious stress can be calculated on the basis of linear elasticity. The method shown in Figure 23 can then be combined with these fictitious elastic stresses. It has to be recognized that, under this combination, the stress approach and strain approach will yield different results, since the fictitious elastic stresses are combined with the real cyclic stress-strain diagram.

Predictions using both the stress and the strain approach are listed in Table 8. Both are shown to be very conservative.

For practical applications, where only a conservative life estimate is necessary, the combination of fictitious elastic stresses and the method shown in Figure 23 appears to be useful. In recommending this procedure, the author is aware of the limitations involved and, therefore, cautions careful judgment in its use.

Given a choice between the stress approach and the strain approach, the author favors the former because of its better prediction. Also, an extremely conservative life estimate can be made by substituting the theoretical elastic stress concentration factor for the actual plastic stress concentration factor. No such convenient upper limit can be given for the strain approach in Figure 23.

5.3 INFLUENCE OF MEAN STRESS

It was shown in References 1 and 3 that crack initiation occurred later in the zero-to-tension tests than in the completely reversed tests for a given nominal stress amplitude. However, cycles-to-complete-failure of the specimen were less for the zero-tension condition compared to completely reversed.

If the methods discussed previously for the completely reversed case are applied to the zero-to-tension case, the prediction will turn out to be safer than in the completely reversed case. Therefore, these methods can be used for zero-to-tension loading at room temperature and 550°F.

A reasonably safe method of predicting low-cycle fatigue life in the presence of stress raisers can therefore be recommended as a result of this study. The method is, in essence, a maximum strain amplitude criterion for crack initiation, and the approximations involved appear to be of a conservative nature. However, an exact life calculation procedure could not be developed from this study.

The approximations involved are considerable and, therefore, research should continue in this area. One point deserves immediate attention—the development of methods for calculating the cycle-dependent variation of the notch-root strain range as it is observed during cyclic plastic straining (see Figure 6). Once this capability is developed, a more accurate life prediction will be possible.

6. CONCLUSIONS

Analysis of the test results of this study led to the development of an approximate, reasonably conservative calculation procedure to analyze the low-cycle fatigue life-to-crack initiation (0.005 - 0.015 inch long crack) of notched specimens under load-controlled conditions. In this method, it is necessary to know the applied nominal mean stress and stress amplitude calculated on an elastic basis, the theoretical elastic uniaxial stress concentration factor of the discontinuity, and the unnotched low-cycle fatigue properties of the material at the operating temperature (which must be below the so-called creep range). The smooth-bar properties required include the cyclic stress-strain diagram and cycles-to-failure data. The variation of the stress and strain concentration factor with applied nominal stress amplitude is then determined with the cyclic stress-strain diagram for the K_t value of interest. Theoretical calculations are involved in this step, and in this study the Stowell method was employed. In Reference 10 the Neuber method was used.

The procedure outlined above was checked against the experimental data obtained in this program and the following results were obtained:

a. Push-pull tests (nominal stresses are statically determinate).

   1. Completely Reversed Condition 550°F
      A slightly unconservative prediction of the life-to-crack initiation was obtained. The degree of unconservative prediction was considered to be acceptable in view of the long crack propagation life.

   2. Room Temperature
      The same degree of unconservative prediction is expected as at 550°F. Figures 17 – 20 indicate some difference between the stress and strain concentration factor and the fatigue strength reduction factor for all the K_t values. Therefore, the method can be applied for all the theoretical elastic stress concentration factors studies in this report.

   3. Influence of Mean Stress
      The life-to-crack initiation for zero-to-tension loading in push-pull at room temperature and 550°F can be calculated in the same way as for completely reversed loading. The results are then expected to be more conservative for zero-to-tension than for the completely reversed case. At the same stress amplitude, crack initiation occurs later in zero-to-tension than in completely reversed loading.

   4. Influence of State-of-Stress
      No difference in crack initiation life was observed between the grooved cylinder and flat plate specimens with a $K_t = 3.3$ at room temperature and 550°F. It appears, therefore, that any influence of the state-of-stress in the two types of specimens was below the resolution of the experiments. Thus, it may be justified to neglect the influence of the state-of-stress in these approximate calculations.

b. Bend tests at room temperature (nominal stress is statically indeterminate). The life prediction was conservative if fictitious elastic stresses were used. It is for this reason that this method appears to be useful for design applications in which a conservative, but not accurate, prediction method is sufficient.

c. All the conclusions were derived for cyclic strain hardening materials. Considerable uncertainties exist about the applicability of the approach for cyclic strain softening materials.

d. It does not appear to be feasible, at the moment, to devise an accurate prediction method. Further work is necessary before such a method can be devised for low-cycle fatigue.

7. ILLUSTRATIONS

This section contains Tables 1 through 8 and Figures 1 through 23.

Table 1. PARAMETERS INVESTIGATED

	Room Temperature							550°F	
	Grooved Cylinders								
	Completely Reversed				Zero to Tension	Flat Plates Zero-to-Tension	Bending Completely Reversed	Grooved Cylinders Completely Reversed	Flat Plates Zero-to-Tension
Material	K_t=1.3	K_t=1.9	K_t=2.5	K_t=3.3	K_t=2.9	K_t=3	K_t=1.8	K_t=3.3	K_t=3
Carbon Steel	–	X	–	X	X	X	–	X	X
2-1/4 Cr–1 Mo Alloy Steel	X	X	X	X	X	X	X	X	X
304 Stainless Steel	–	X	X	X	X	X	X	X	X

NOTE: X in table means that this parameter was studied.
All tests under load control.
K_t = uniaxial, theoretical, elastic stress concentration factor.

Table 2. CONTENTS OF PREVIOUS REPORT

Subject	Data Reported In
Objective of program, specimen design, identification of material used for testing.	GEAP-4911, 1965 (Quarterly Progress Report No. 1)
Mechanical properties of test material at room temperature, microstructure, Charpy impact. Low-cycle fatigue (LCF) data of smooth bars.	GEAP-4964, 1965 (No. 2)
Complete room-temperature smooth-bar LCF data.	GEAP-5082, 1965 (No. 3)
Test results, flat plates , $K_t = 3$.	GEAP-5147, 1966 (No. 4)
Quality assurance of strain gages used.	GEAP-5147, Appendix C
Preliminary analysis of flat plates, $K_t = 3$.	GEAP-5192, 1966 (No. 5)
Crack growth data, flat plates, $K_t = 3$.	GEAP-5279, 1966 (No. 6)
Initial tests, flat plates, $K_t = 3$ at 550°F.	GEAP-5427, 1966 (No. 7)
LCF strength reduction in notched flat plates (topical report)	GEAP-5410, 1967
Complete description of mechanical behavior of smooth bar specimens, cyclic, monotonic $\sigma - \epsilon$ diagram, strain hardening exponent, room temperature.	GEAP-5474, Appendix B, 1967, (No. 8)
550°F tests, flat plate specimens, $K_t = 3$.	GEAP-5474, 1967 (No. 8)
550°F tensile properties of test materials. Grooved cylinders, $K_t = 2.9$, zero-to-tension, room temperature.	GEAP-5512, 1967 (No. 9)
Test results, grooved cylinders, $K_t = 3.3$, completely reversed, room temperature.	GEAP-5554, 1967 (No. 10)
Test results, grooved cylinders, $K_t = 3.3$, completely reversed, 550°F.	GEAP-5587, 1967 (No. 11)
Test results, grooved cylinders, $K_t = 1.9$, completely reversed, room temperature.	GEAP-5637, 1968 (No. 12)
Test results, bend tests, $K_t = 1.8$, room temperature.	GEAP-5680, 1968 (No. 13)
Cyclic deformation behavior of smooth-bar specimens, 550°F.	GEAP-5716, 1968 (No. 14)
Test results, grooved cylinders, $K_t = 1.3$ and $K_t = 2.5$, room temperature.	GEAP-5770, 1969 (No. 15)

Table 2. (continued)

Subject	Data Reported In
Stress controlled, smooth-bar data, ratcheting, room temperature.	GEAP-10024, 1969 (No. 16)
Influence of stress-strain concentration and mean stress on the LCF behavior of the three structural steels at room temperature (topical report).	GEAP-5726, 1968
Notched high-strain fatigue behavior of three low-strength structural steels (topical report).	GEAP-5714, 1969
The 550°F notched high-strain fatigue behavior of three low-strength structural steels (includes smooth-bar data, cyclic stress-strain diagram) (topical report).	GEAP-10090, 1969

Table 3
ROOM TEMPERATURE AND 550°F TENSILE PROPERTIES OF THREE PIPING MATERIALS

Material	Temp. (°F)	Prop. Limit (10^3 psi)	0.2% YS (10^3 psi)	UTS (10^3 psi)	RA (%)	Elong. (2 in. Gage Length) (%)
Carbon Steel	75	21.0	29.4	62.4	55.8	35.8
	550	–	–	72.0	47.0	30.0
	550	15.5	29.5	72.1	49.0	31.0
	550	11.5	25.5	72.5	45.0	29.0
2-1/4 Cr–1 Mo Alloy Steel	75	23.6	36.7	74.6	67.5	31.5
	550	18.0	32.0	69.5	59.0	23.0
	550	24.0	32.0	69.5	58.0	21.0
	550	–	–	70.1	58.0	20.0
Type 304 Stainless Steel	75	26.9	38.8	85.0	76.1	66.8
	550	–	–	68.5	70.0	45.0
	550	15.0	24.0	67.0	70.0	50.0
	550	14.0	25.9	68.0	68.0	46.0

Table 4
CHEMICAL COMPOSITION OF MATERIALS TESTED
(Mill Analysis)

Material	C	Mn	P	S	Si	Ni	Cr	Mo
Low Carbon Steel	0.16	0.65	0.008	0.032	0.22	–	–	–
304 Stainless Steel	0.07	1.45	0.021	0.028	0.53	8.77	19.0	–
2-1/4 Cr–1 Mo Alloy Steel	0.12	0.54	0.010	0.015	0.31	–	2.39	1.00

Table 5
NOMINAL STRESSES CALCULATED FOR THE BEND TESTS

Material	Load Ampl. (10^4 lb)	Nom. Stress Ampl. Based on Mc/I (10^3 psi)	Nom. Stress Ampl. Based on Cyclic $\sigma - \epsilon$ Diagram (10^3 psi)	N_C, Number of Cycles to Crack Initiation
2-1/4 Cr–1 Mo	1.0	45.4	37	2350
2-1/4 Cr–1 Mo	1.2	54.5	41	1050
304 Stainless Steel	1.0	45.4	33	2220
304 Stainless Steel	1.2	54.5	37	946

Table 6

COMPARISON OF PREDICTED AND OBSERVED LIVES-TO-CRACK INITIATION.
GROOVED CYLINDERS, K_t = 3.3, COMPLETELY REVERSED LOAD CONTROL (550°F)
MATERIAL: CARBON STEEL

Nom. Stress Amplitude (10^3 psi)	Calculated Steady-State Notch-Root Strain Range (%)	Predicted Life-to-Crack Initiation (Cycles)	Observed Life-to-Crack Initiation (Cycles)	Observed Life-to-Failure (Cycles)
25	0.75	7200	4500	3.8×10^4
30	0.95	3800	1800	2.3×10^4
35	1.19	1850	680	1.5×10^4
40	1.48	900	*180	$*10^4$

* Extrapolated value

Table 7

COMPARISON OF PREDICTED AND OBSERVED LIVES-TO-CRACK INITIATION.
GROOVED CYLINDERS, K_t = 3.3, COMPLETELY REVERSED LOAD CONTROL (550°F)
MATERIAL: 2-1/4 Cr–1 Mo ALLOY STEEL

Nom. Stress Amplitude (10^3 psi)	Calculated Steady-State Notch-Root Strain Range (%)	Predicted Life-to-Crack Initiation (Cycles)	Observed Life-to-Crack Initiation (Cycles)	Observed Life-to-Failure (Cycles)
20	0.76	5800	*12,500	10^5
25	1.00	3350	4,300	8.6×10^4
30	1.50	1500	1,500	3.9×10^4
35	1.80	1050	500	1.85×10^4
40	*2.40	600	180	8500

* Extrapolated value

Table 8

PREDICTION OF FATIGUE LIFE-TO-CRACK INITIATION FOR BEND TESTS.
ROOM TEMPERATURE,COMPLETELY REVERSED, LOAD-CONTROLLED CONDITION, $K_t = 1.8$
MATERIAL: 2-1/4 Cr–1 Mo Alloy Steel

Nominal Stress Ampl. (10^3 psi)	Calculated Steady State Notch-Root Strain Range (%)	Predicted Life-to-Crack-Initiation (Cycles)	Observed Life-to-Crack-Initiation (Cycles)
	Nominal Stress Based on Elasto-Plastic Analysis		
42.5	1.40	1700	700
40.0	1.04	3100	1050
37.5	0.96	3700	2200
35.0	0.86	4600	3800
	Nominal Stress Based on Elastic Analysis		
Stress Approach			
50.0	2.65	500	1030
47.5	2.15	730	1700
45.0	1.80	1050	2500
Strain Approach			
50.0	3.75	350	1030
47.5	3.10	360	1700
45.0	2.40	600	2500

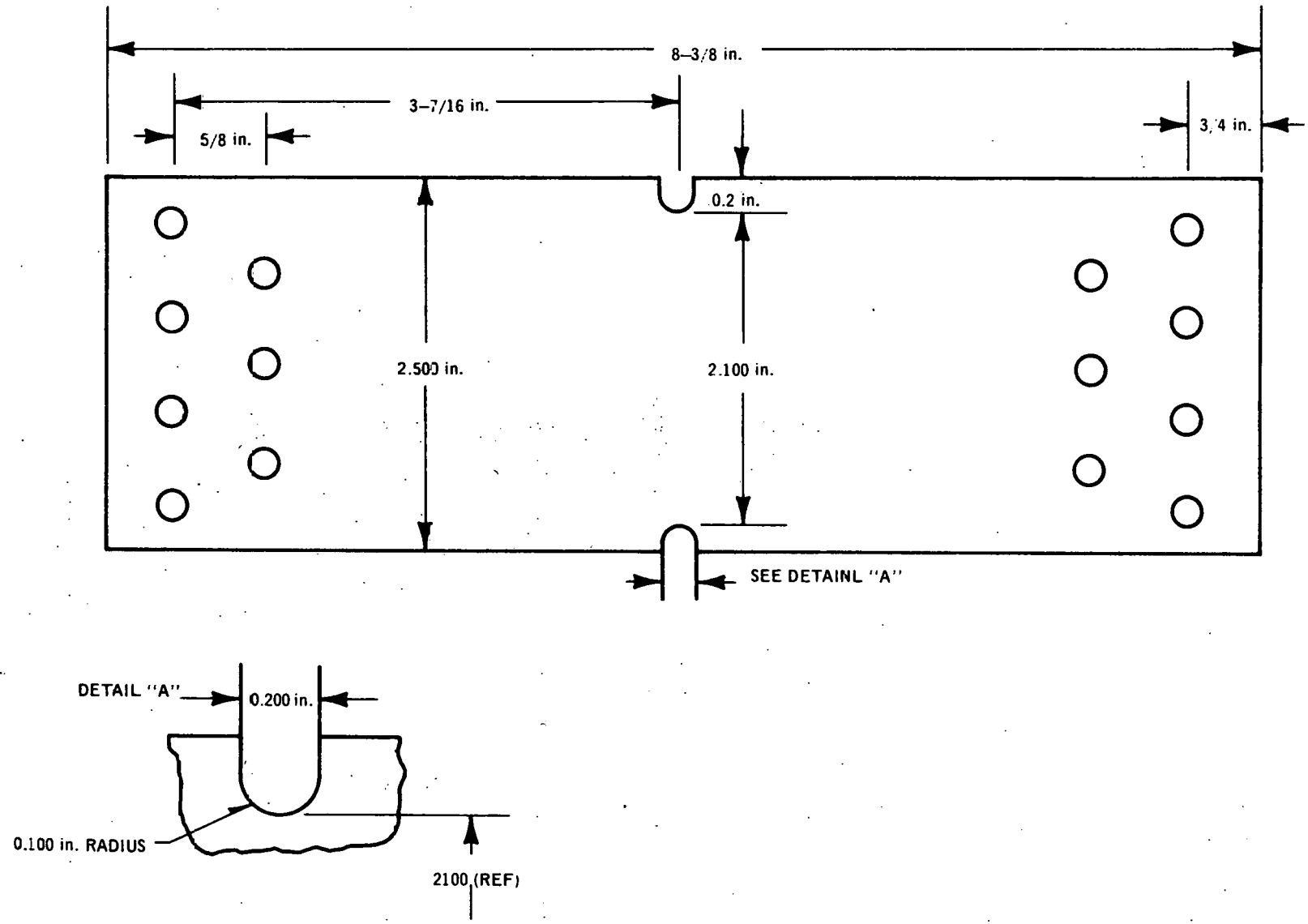

Figure 1. Flat Plate Specimen

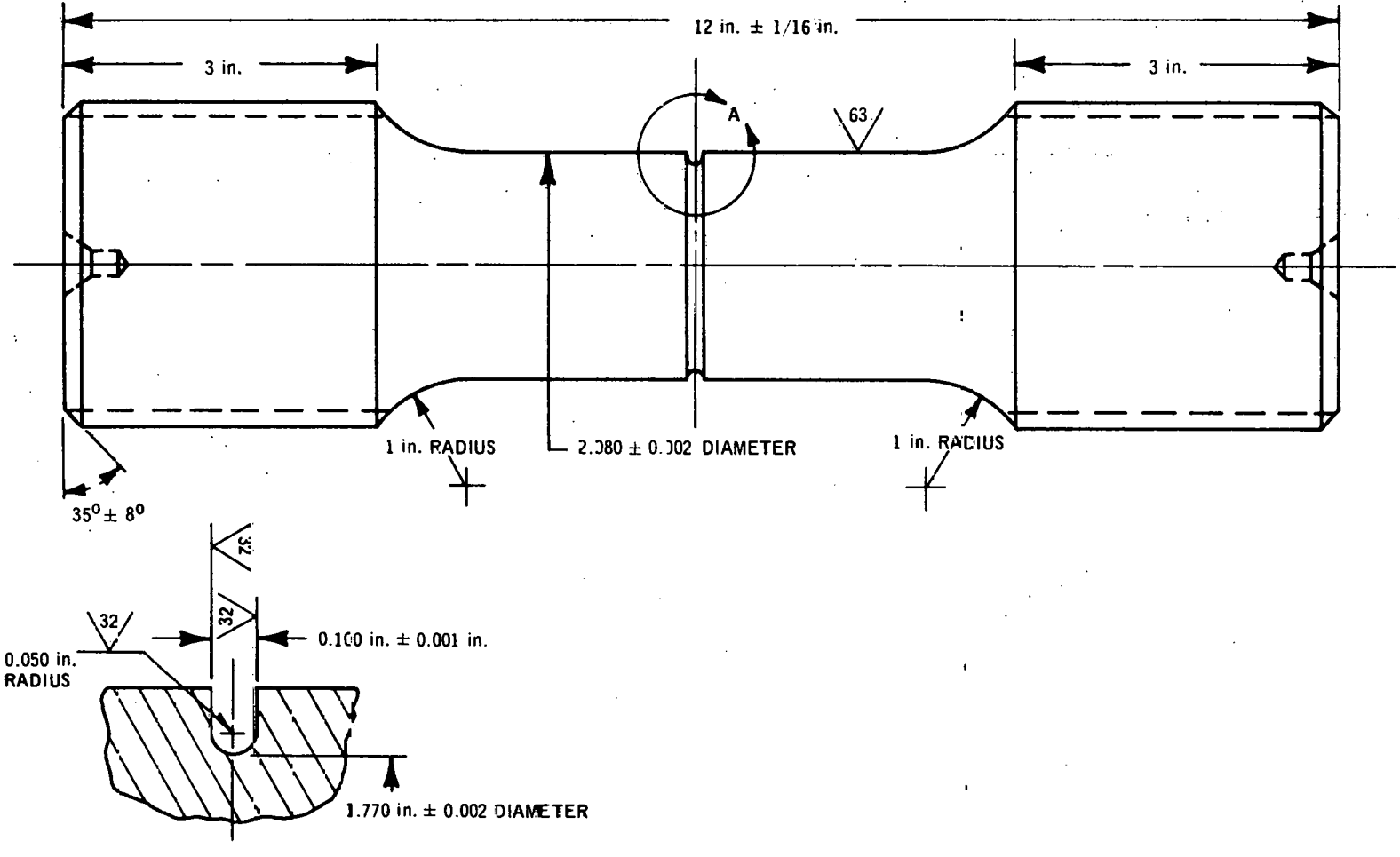

Figure 2. Grooved Cylinder Specimen

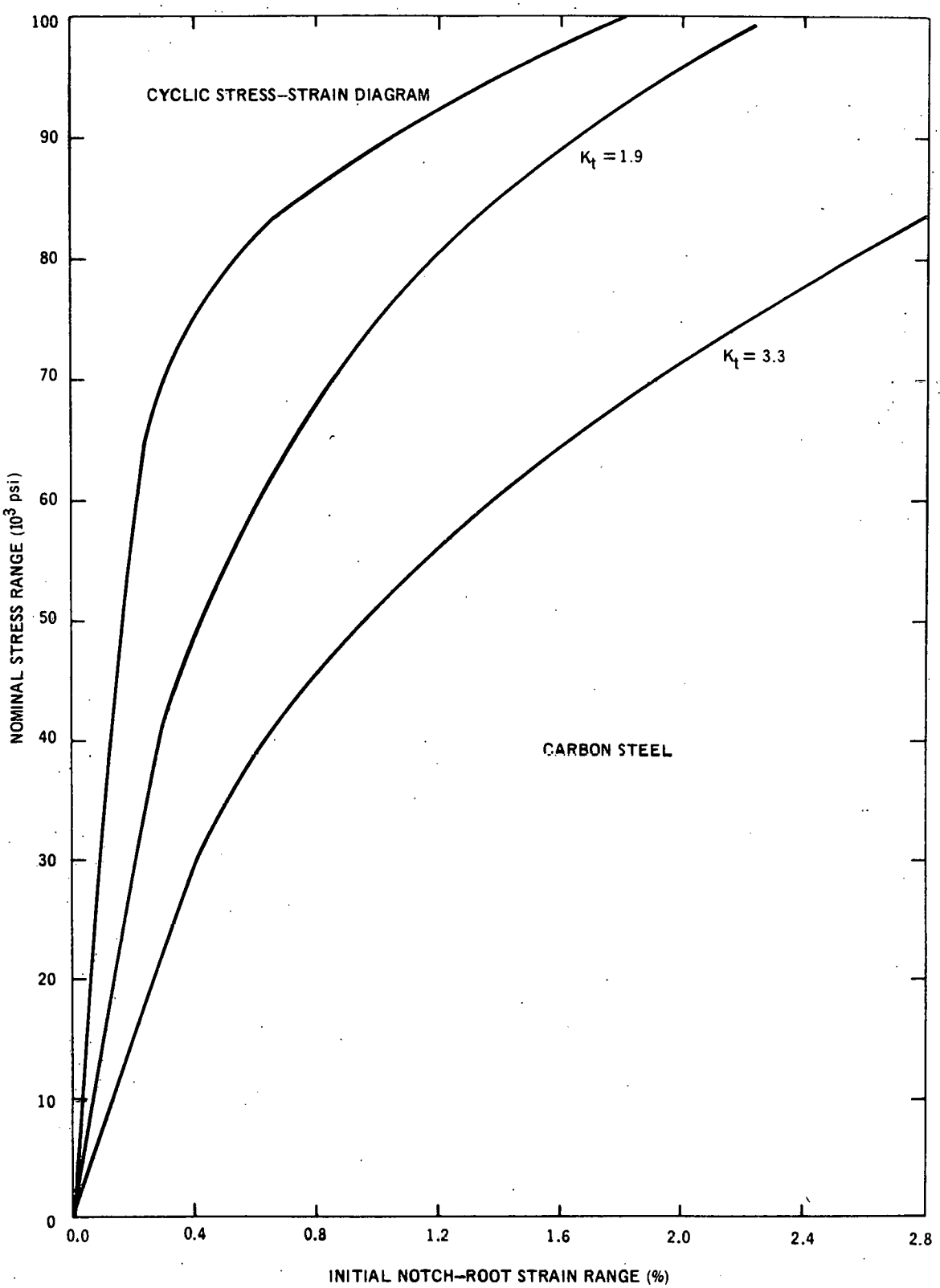

Figure 3. *Initial Notch-Root Strain Range Nominal Stress Range Diagrams for the Different K_t Values Indicated. Grooved Cylinders, Completely Reversed, Load Control (Room Temperature). Material: Carbon Steel.*

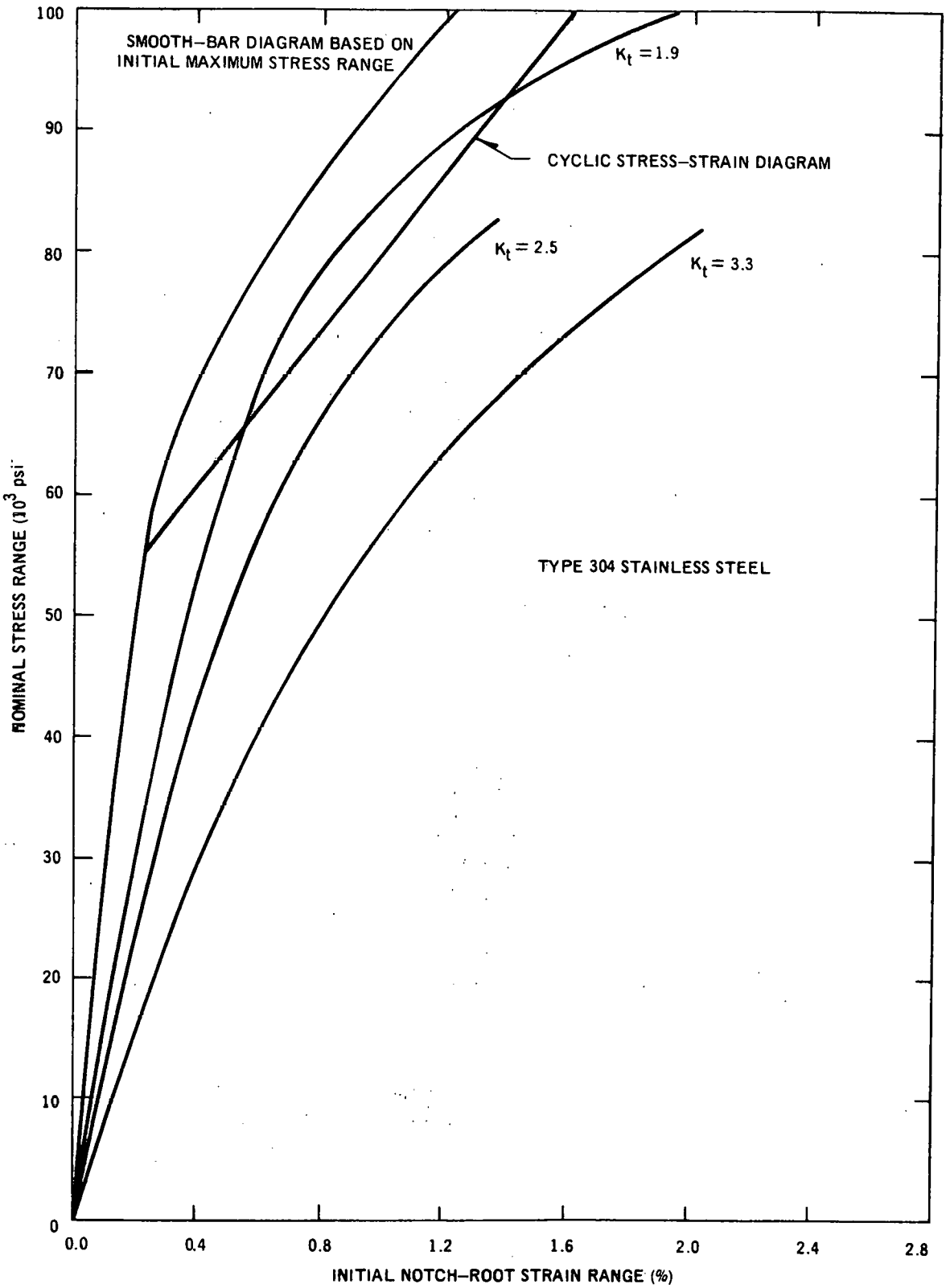

Figure 4. *Initial Notch-Root Strain Range Nominal Stress Range Diagrams for the Different K_t Values Indicated. Grooved Cylinders, Completely Reversed, Load Control (Room Temperature). Material: Type 304 Material: Type 304 Stainless Steel.*

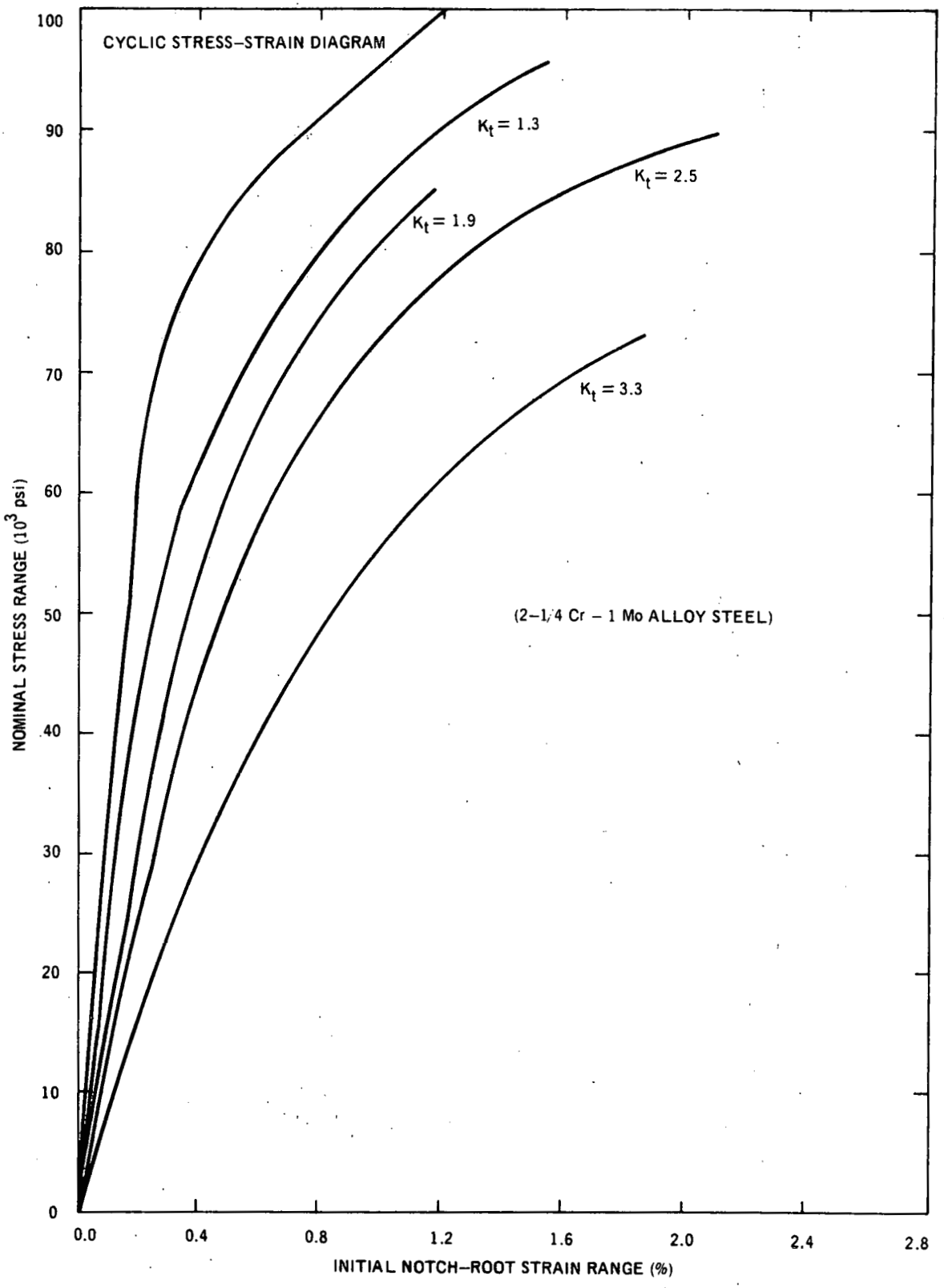

Figure 5. *Initial Notch-Root Strain Range Nominal Stress Range Diagrams for the Different K_t Values Indicated. Grooved Cylinders, Completely Reversed, Load Control (Room Temperature). Material: 2-1/4 Cr–1 Mo Alloy Steel.*

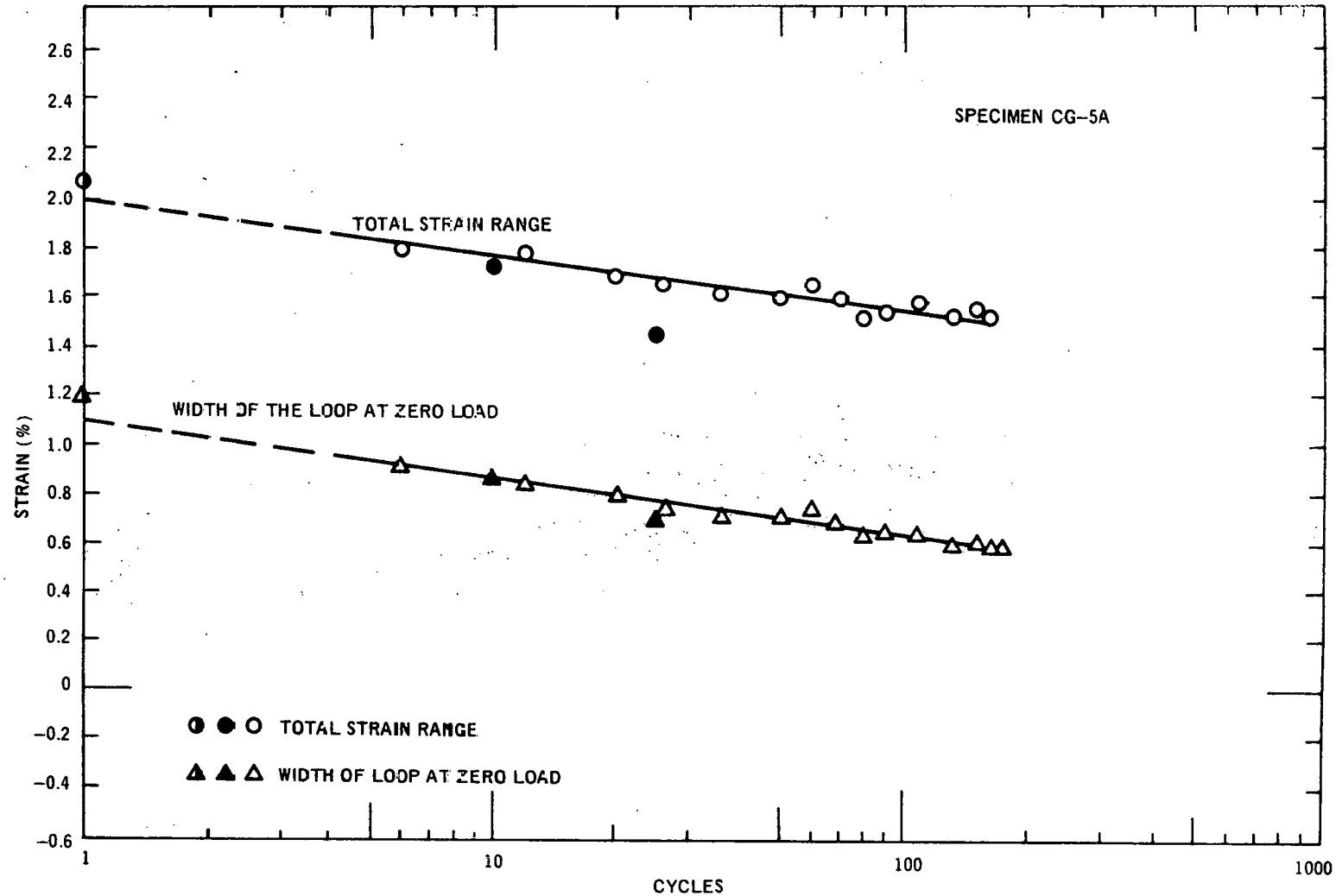

Figure 6. *Continuous Decrease of Notch-Root Strain Range During Cycling at High Nominal Stresses. Grooved Cylinder, $K_t = 3.3$, $\sigma_a = 35 \times 10^3$ psi Completely Reversed Loading. Material: Carbon Steel.*

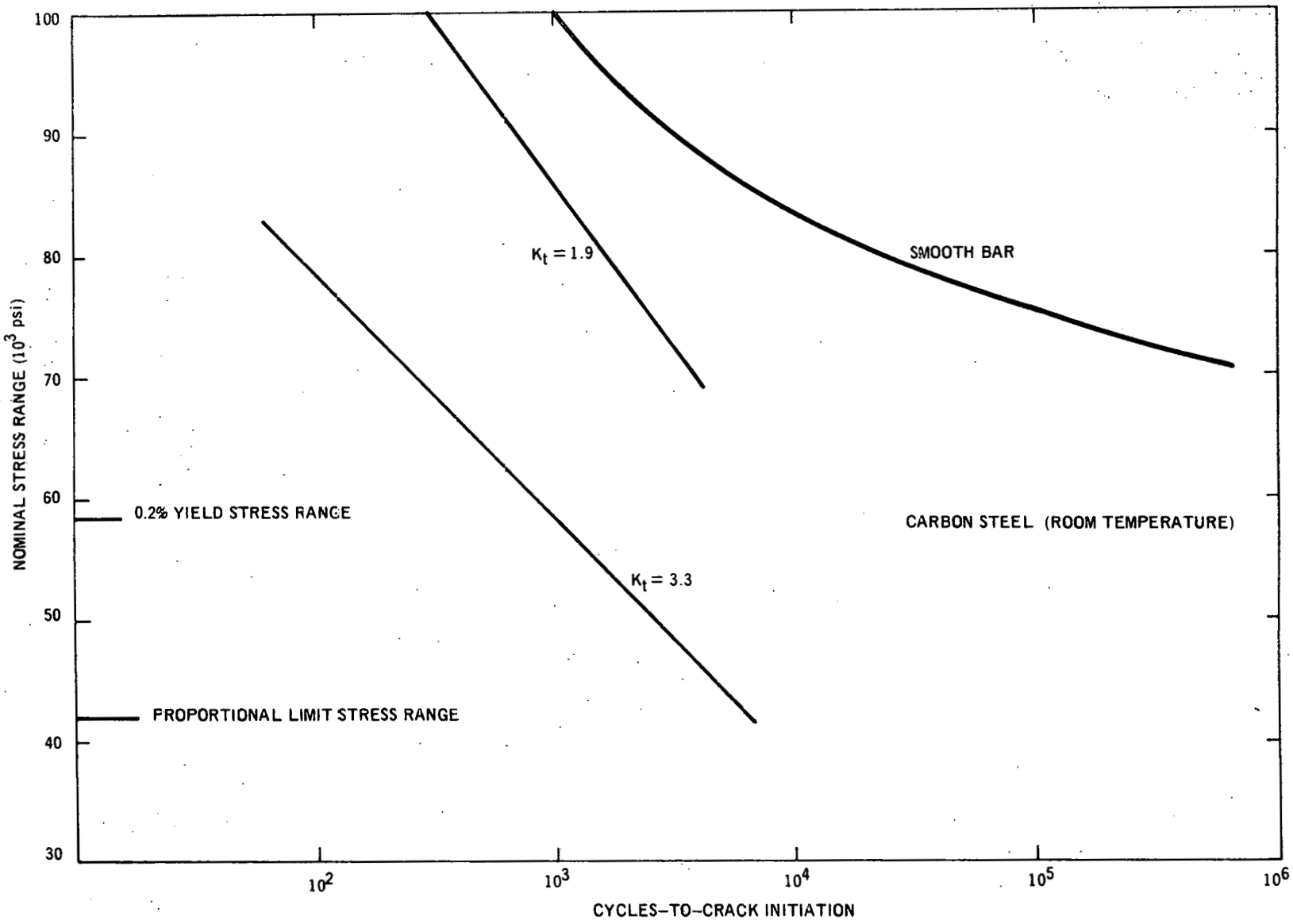

Figure 7. Nominal Stress Range Versus Cycles-to-Crack Initiation for Different Values of K_t. Smooth-Bar Data are Based on the Steady-State Stress Range. Material: Carbon Steel.

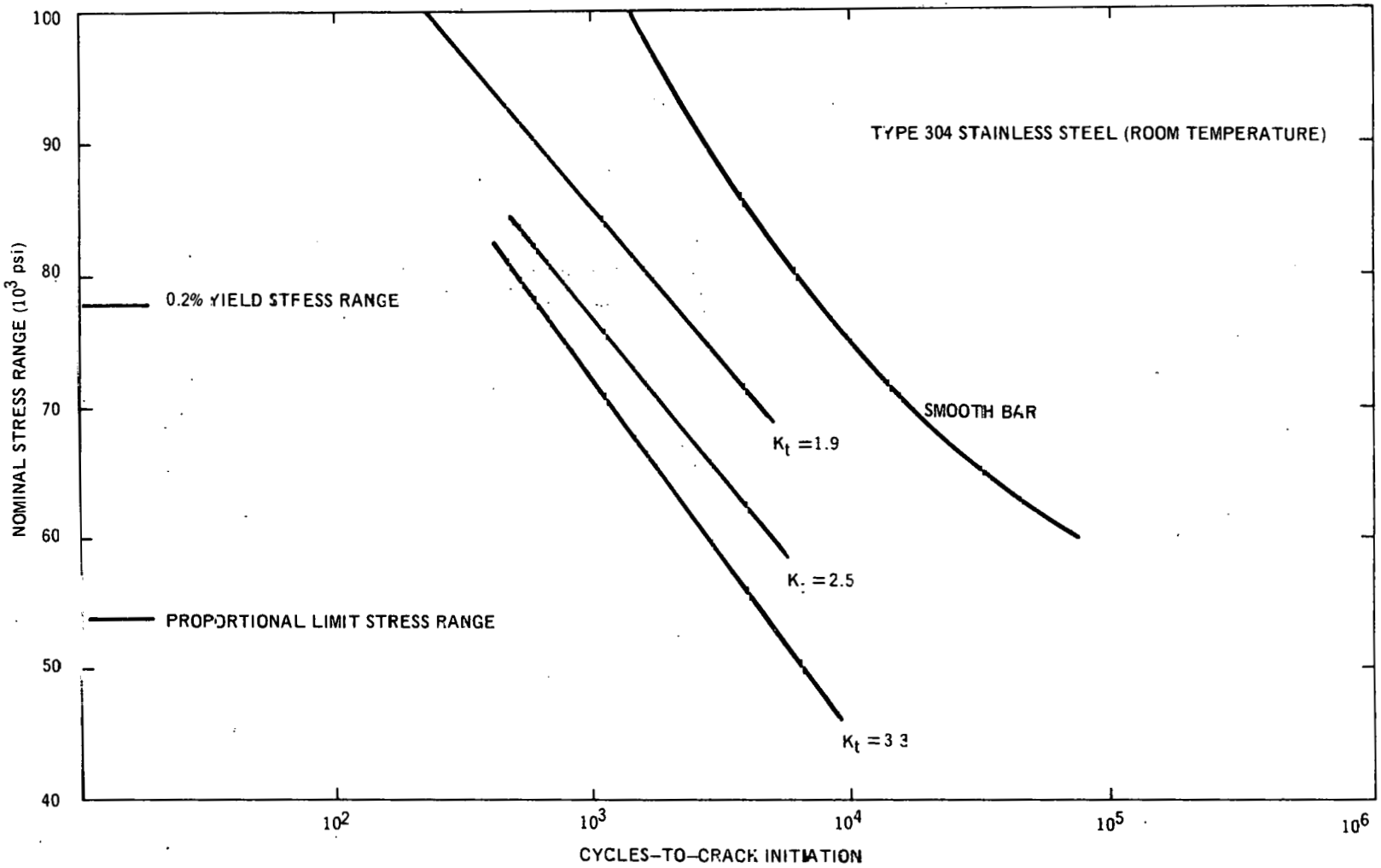

Figure 8. Nominal Stress Range Versus Cycles-to-Crack Initiation for Different Values of K_t. Smooth-Bar Data are Based on the Steady-State Stress Range. Material: Type 304 Stainless Steel.

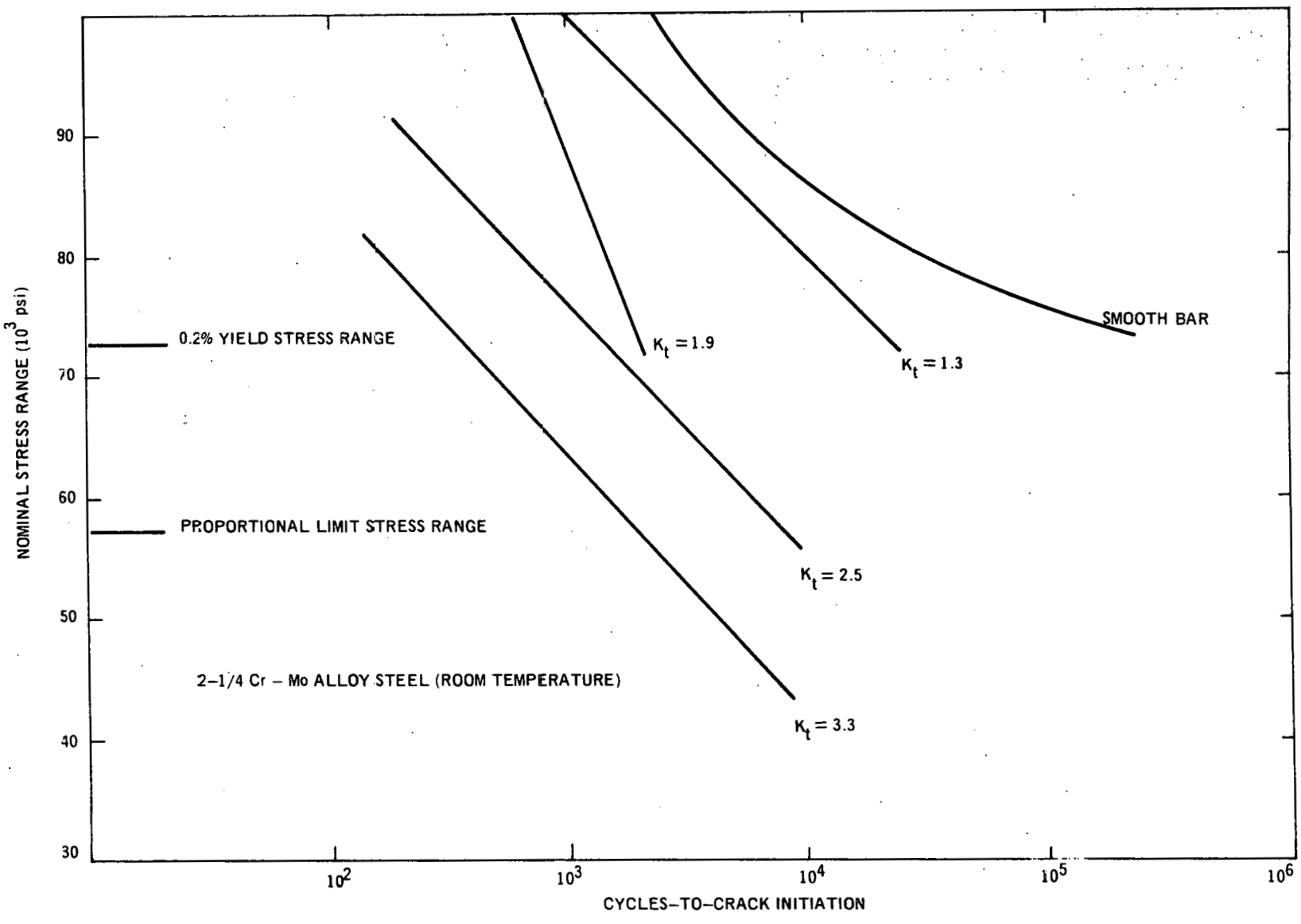

Figure 9. Nominal Stress Range Versus Cycles-to-Crack Initiation for Different Values of K_t. Smooth-Bar Data are Based on the Steady-State Stress Range. Material: 2-1/4 Cr–1 Mo Alloy Steel.

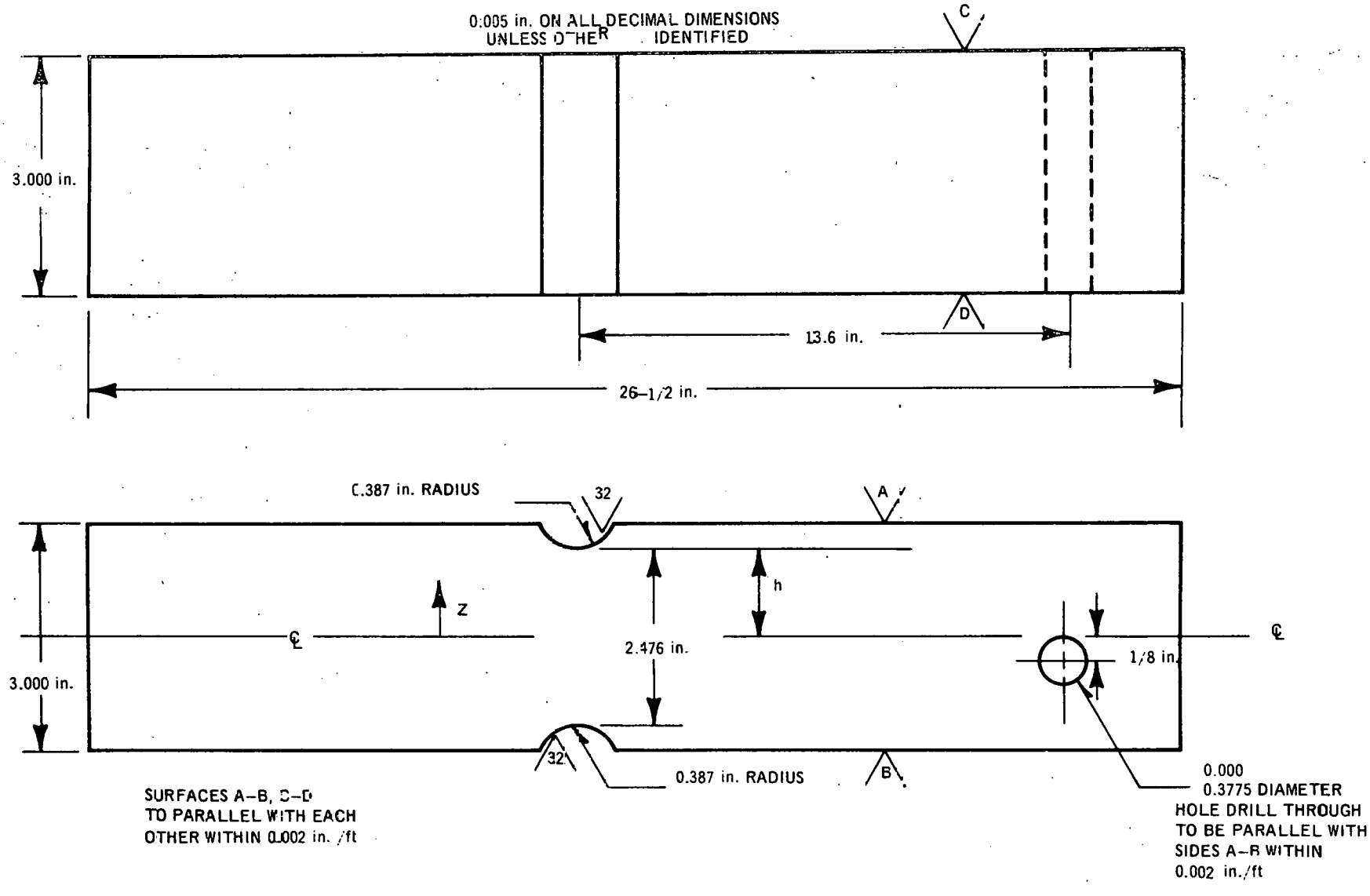

Figure 10. Bending Test Specimen.

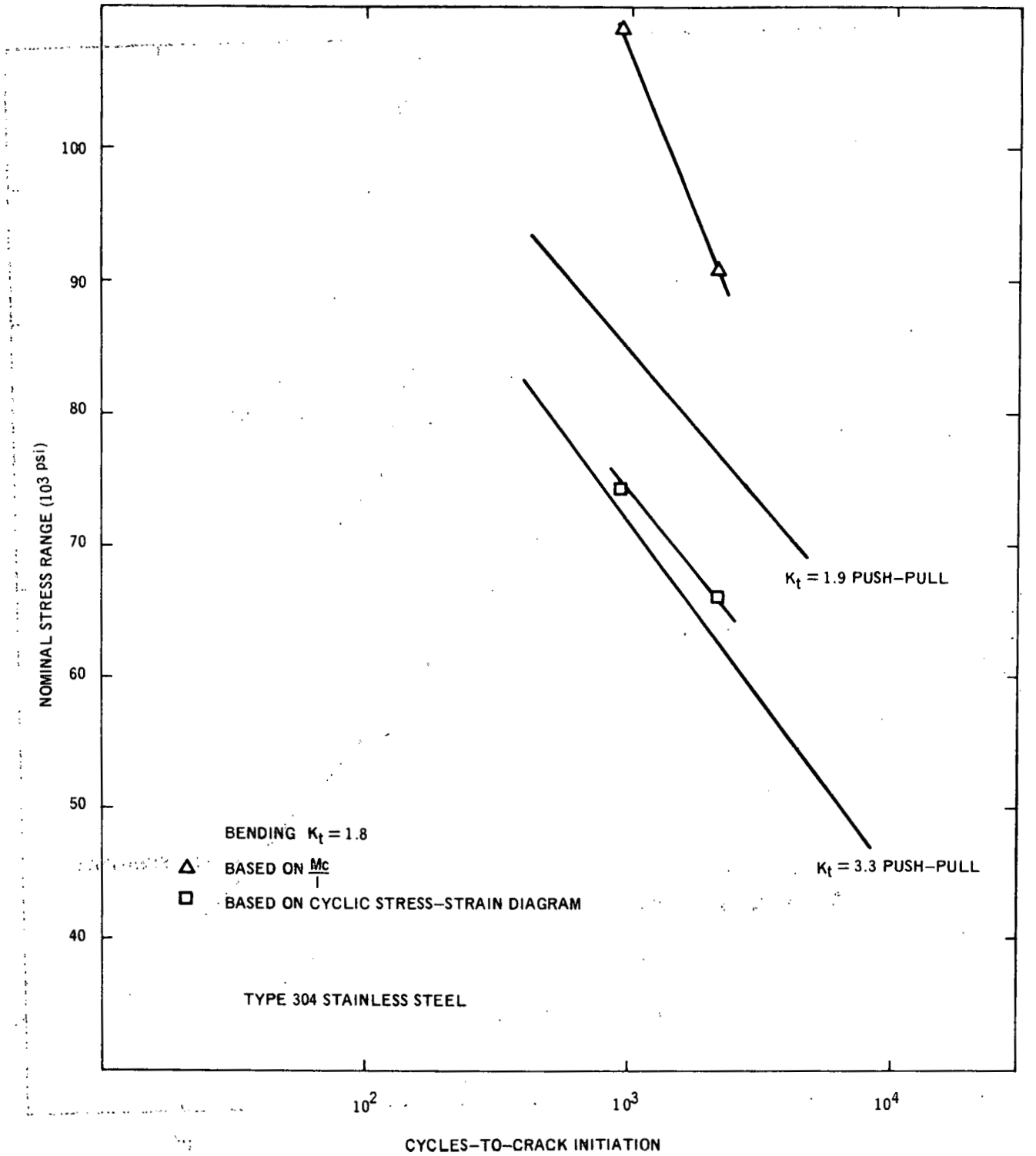

Figure 11. Nominal Stress Range Based on Mc/I and the Nominal Stress Range Derived from an Approximate Elasto-Plastic Analysis Versus Crack Initiation Together with Corresponding Push-Pull Data. Material: Type 304 Stainless Steel.

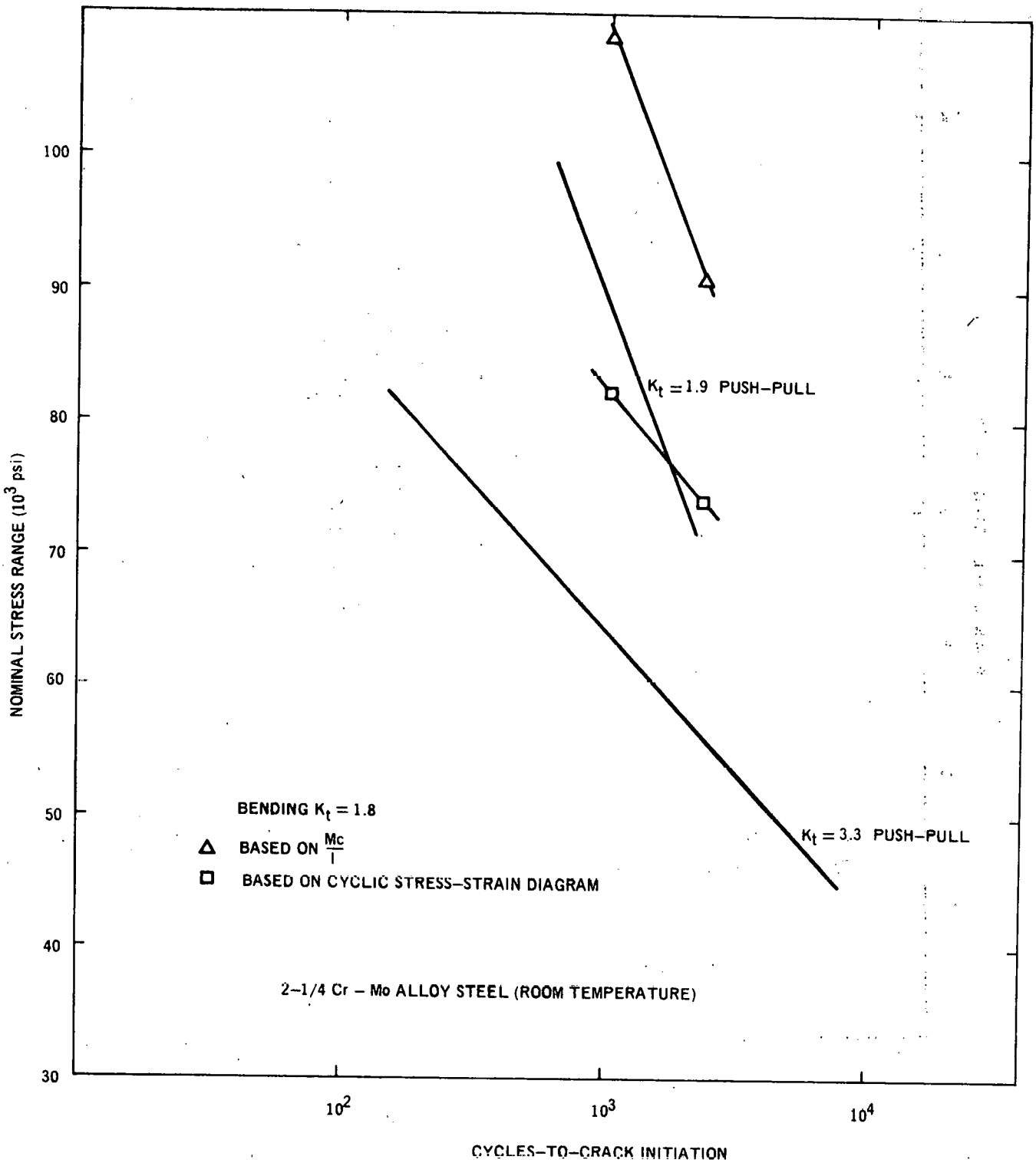

Figure 12. Nominal Stress Range Based on Mc/I and the Nominal Stress Range Derived from an Approximate Elasto-Plastic Analysis Versus Crack Initiation Together with Corresponding Push-Pull Data. Material: 2-1/4 Cr–1 Mo Alloy Steel.

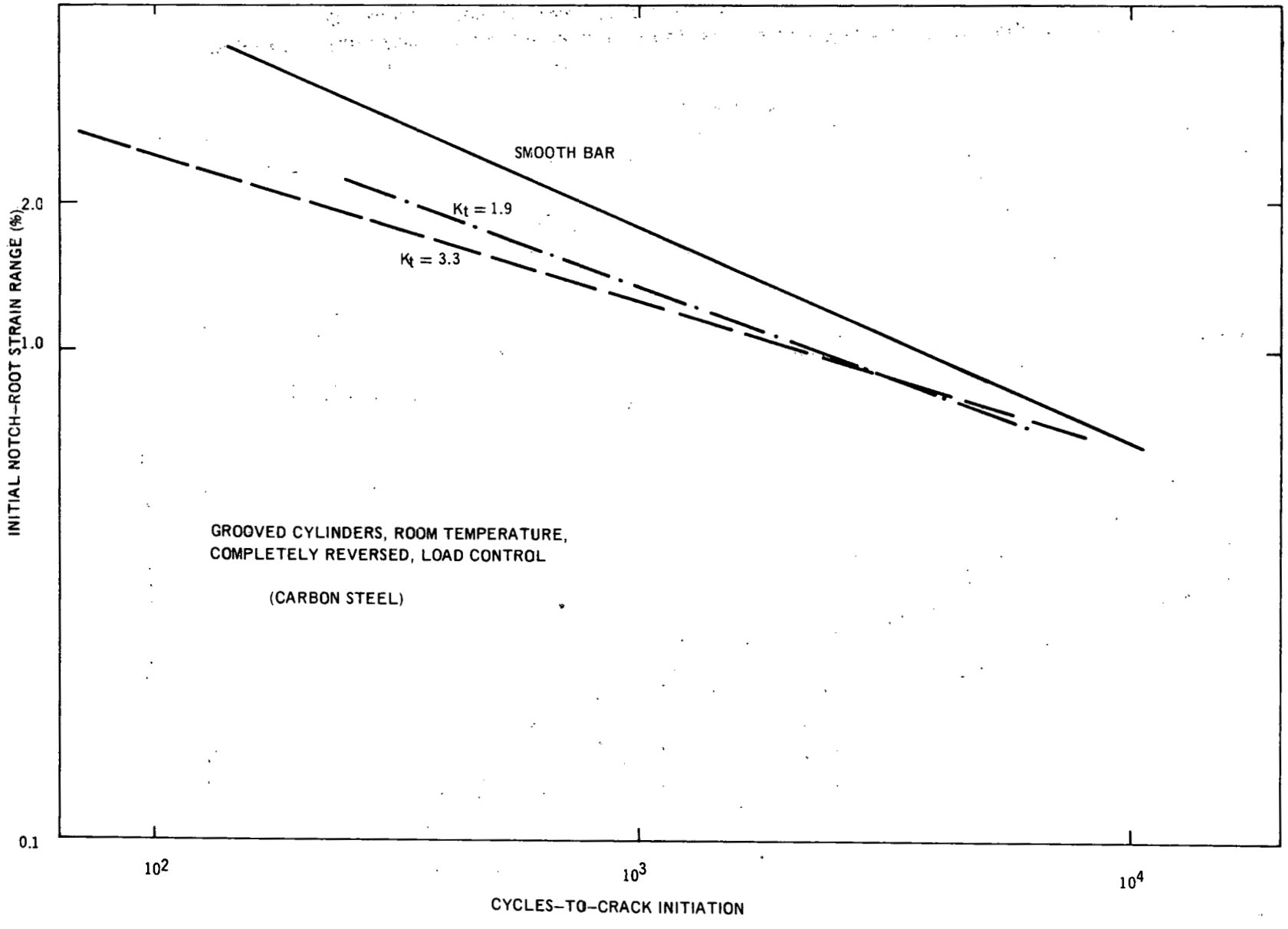

Figure 13. Initial Notch-Root Strain Range Versus Cycles-To-Crack Initiation for Various Degrees of Stress Concentration. Material: Carbon Steel.

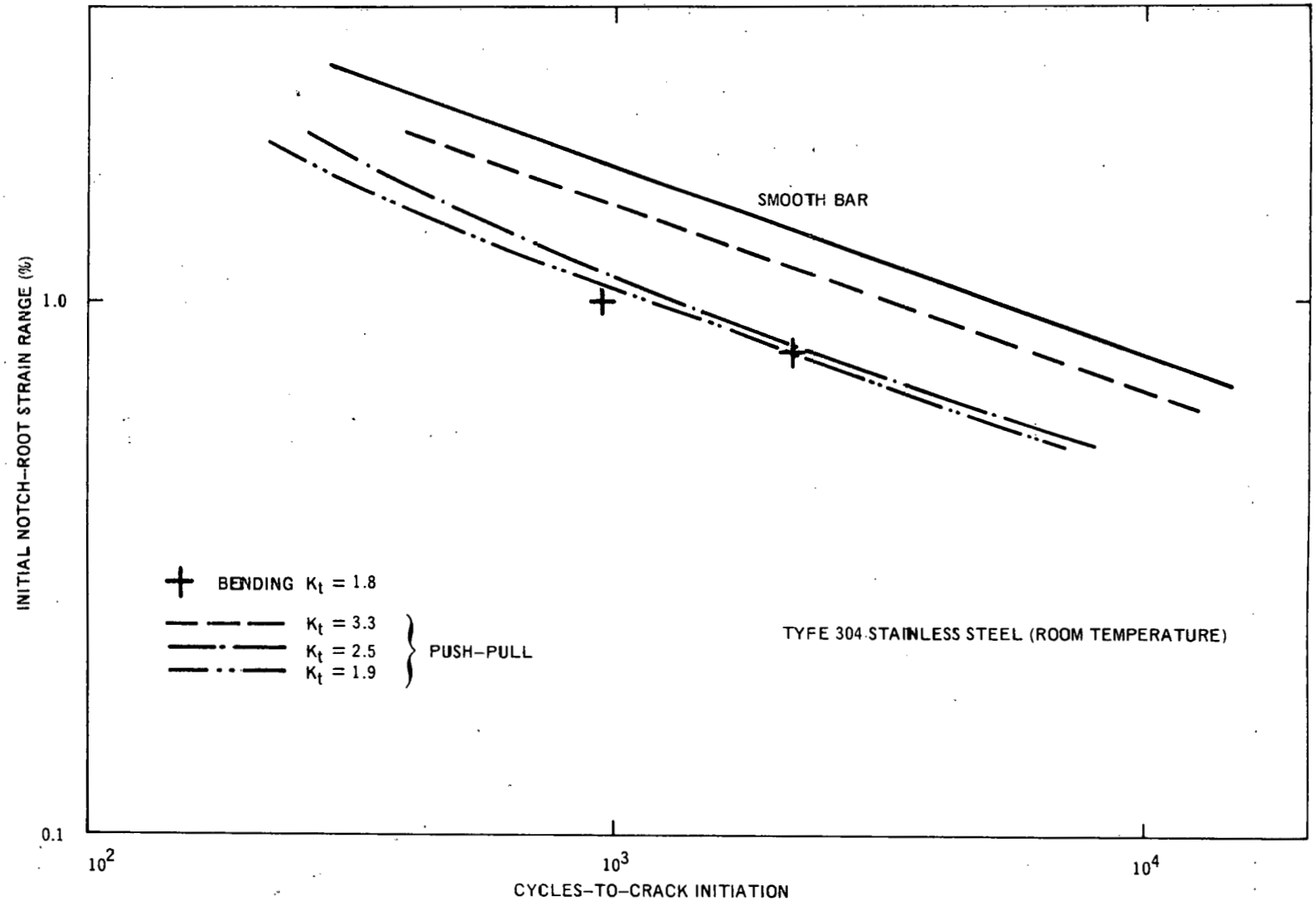

Figure 14. Initial Notch-Root Strain Range Versus Cycles-To-Crack Initiation for Various Degrees of Stress Concentration. Material: Type 304 Stainless Steel.

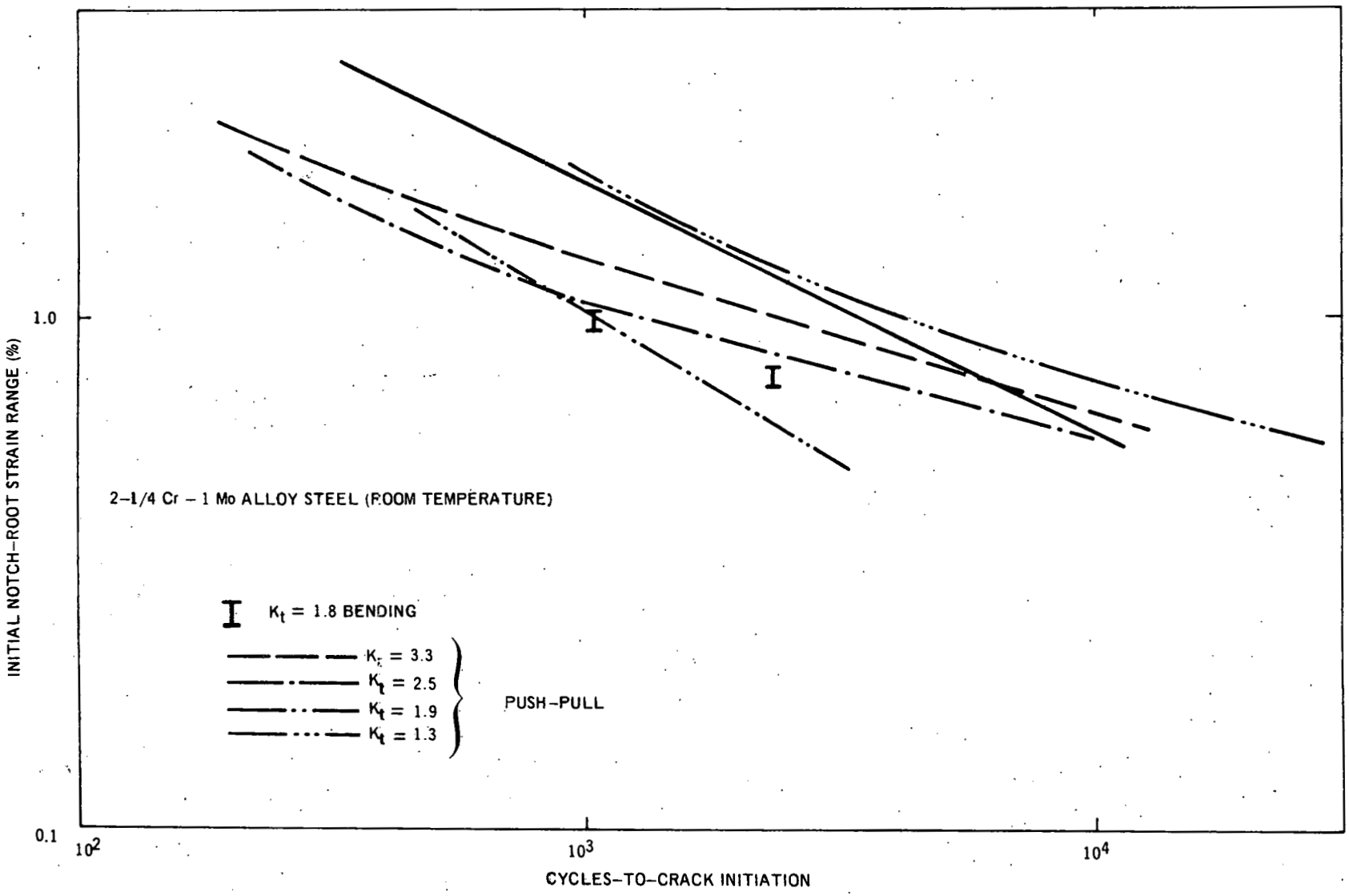

Figure 15. Initial Notch-Root Strain Range Versus Cycles-To-Crack Initiation for Various Degrees of Stress Concentration. Material: 2-1/4 Cr–1 Mo Alloy Steel.

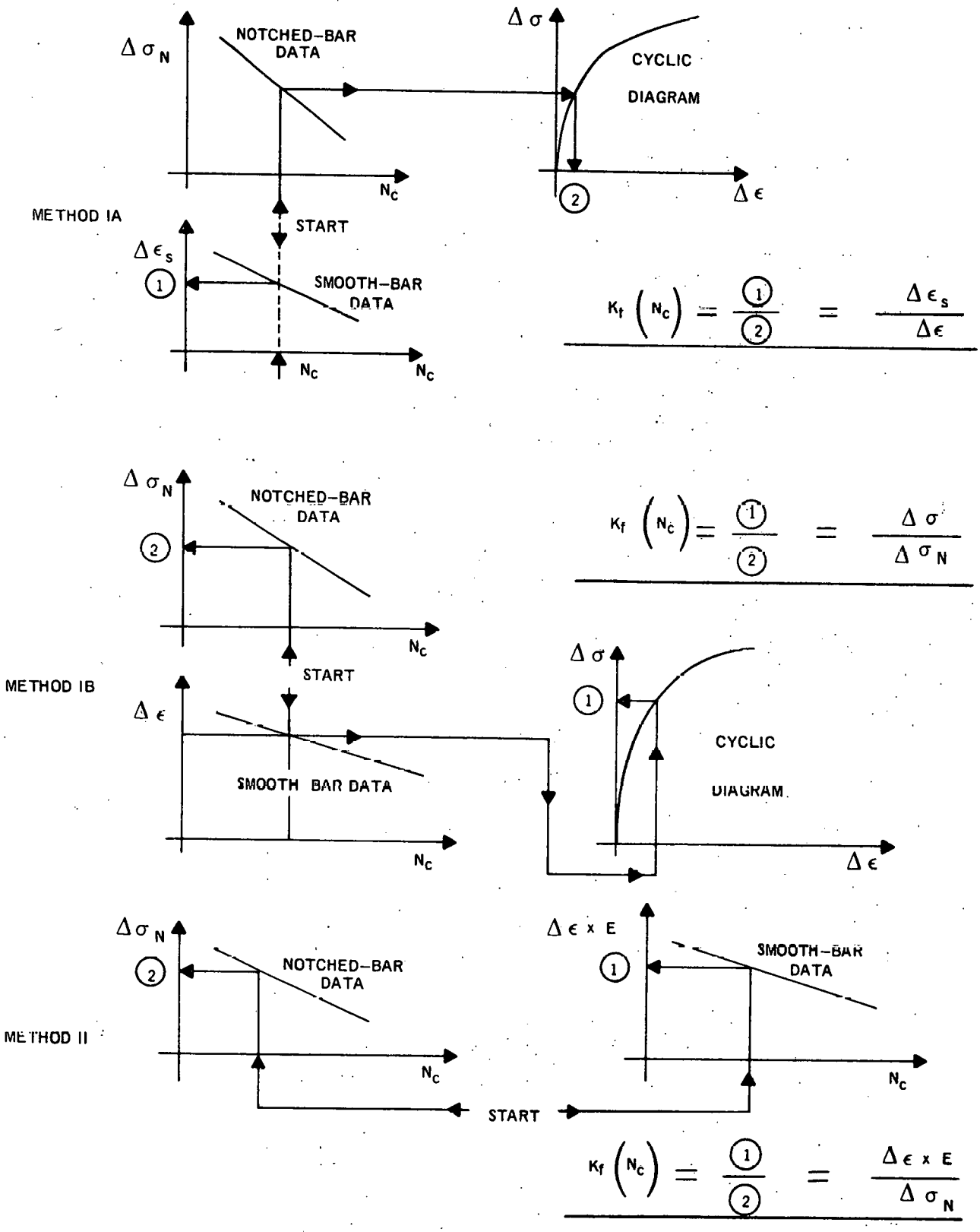

Figure 16. Three Possibilities of Defining the Fatigue Strength Reduction Factor.

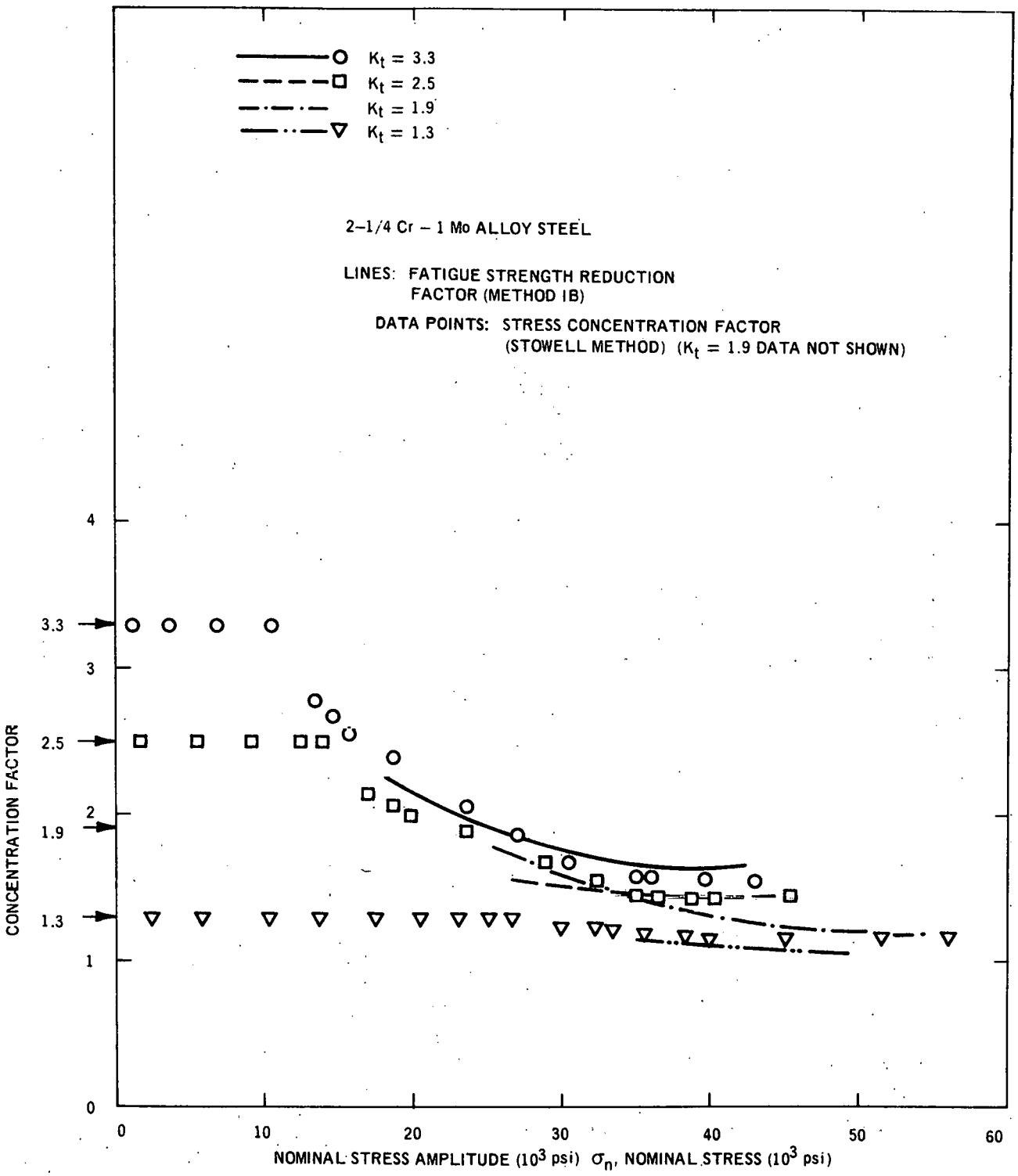

Figure 17. Method IB Factor and Stress Concentration Factor for 2-1/4 Cr–1 Mo Alloy Steel Versus Applied Nominal Stress Amplitude. The Cyclic Stress-Strain Diagram Was Used in the Calculations (Room Temperature).

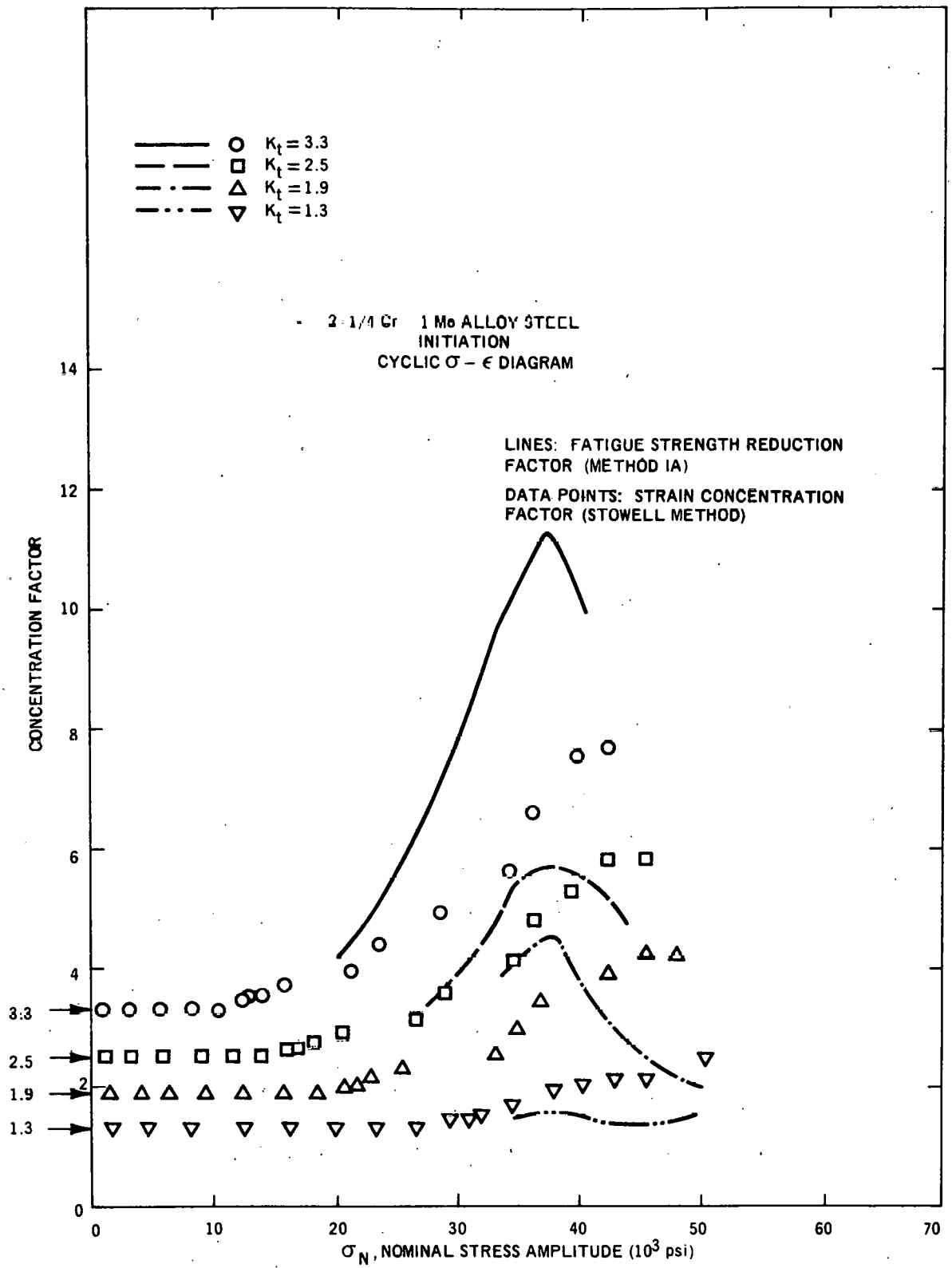

Figure 18. Method IA Factor and Strain Concentration Factor for 2-1/4 Cr–1 Mo Alloy Steel Versus Applied Nominal Stress Amplitude. The Cyclic Stress-Strain Diagram Was Used in the Calculations (Room Temperature).

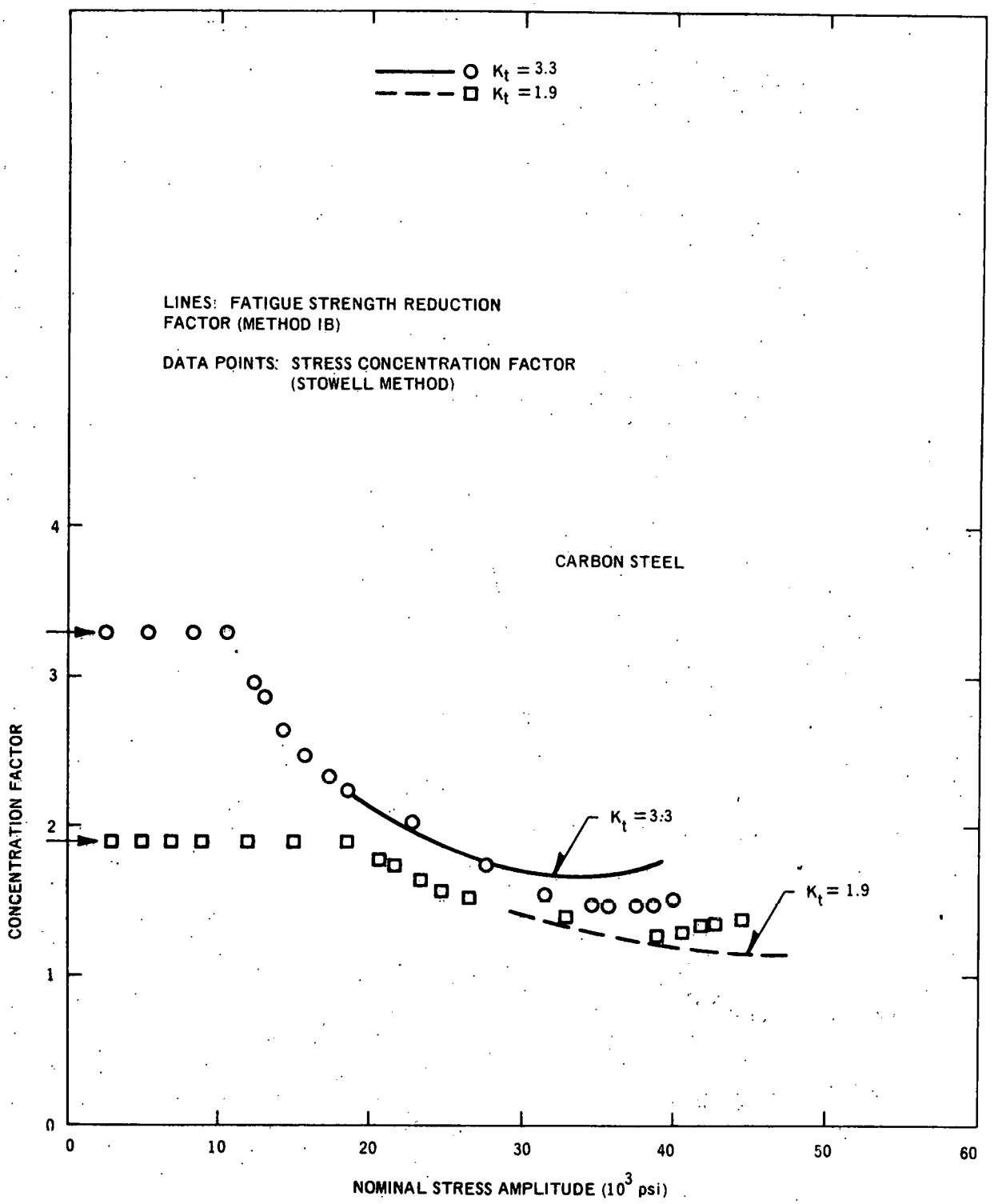

Figure 19. Method IB Factor and Stress Concentration Factor for Carbon Steel Versus Applied Nominal Stress Amplitude. The Cyclic Stress-Strain Diagram was Used in the Calculations (Room Temperature).

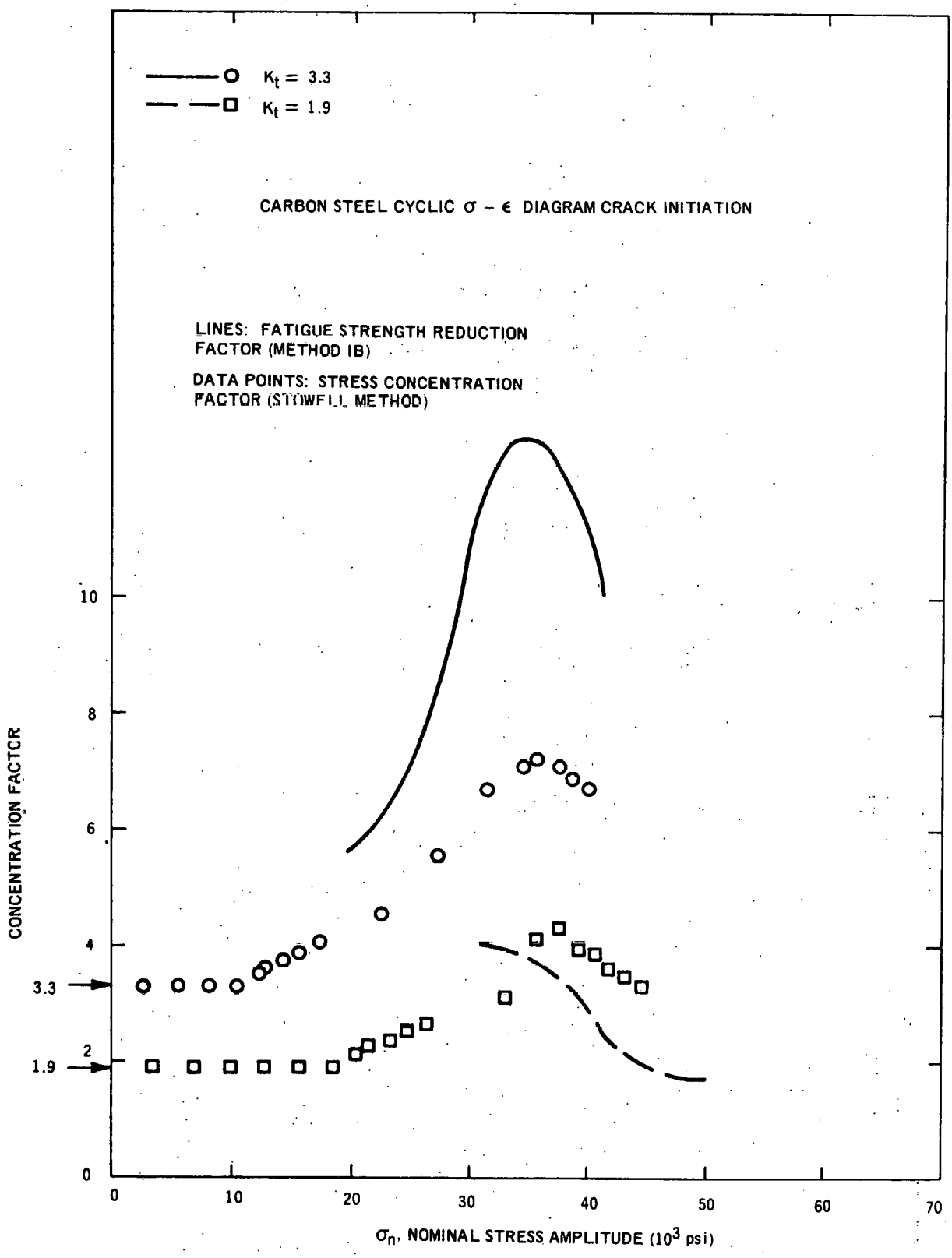

Figure 20. Method IA Factor and Strain Concentration Factor for Carbon Steel Versus Applied Nominal Stress Amplitude. The Cyclic Stress-Strain Diagram Was Used in the Calculations (Room Temperature).

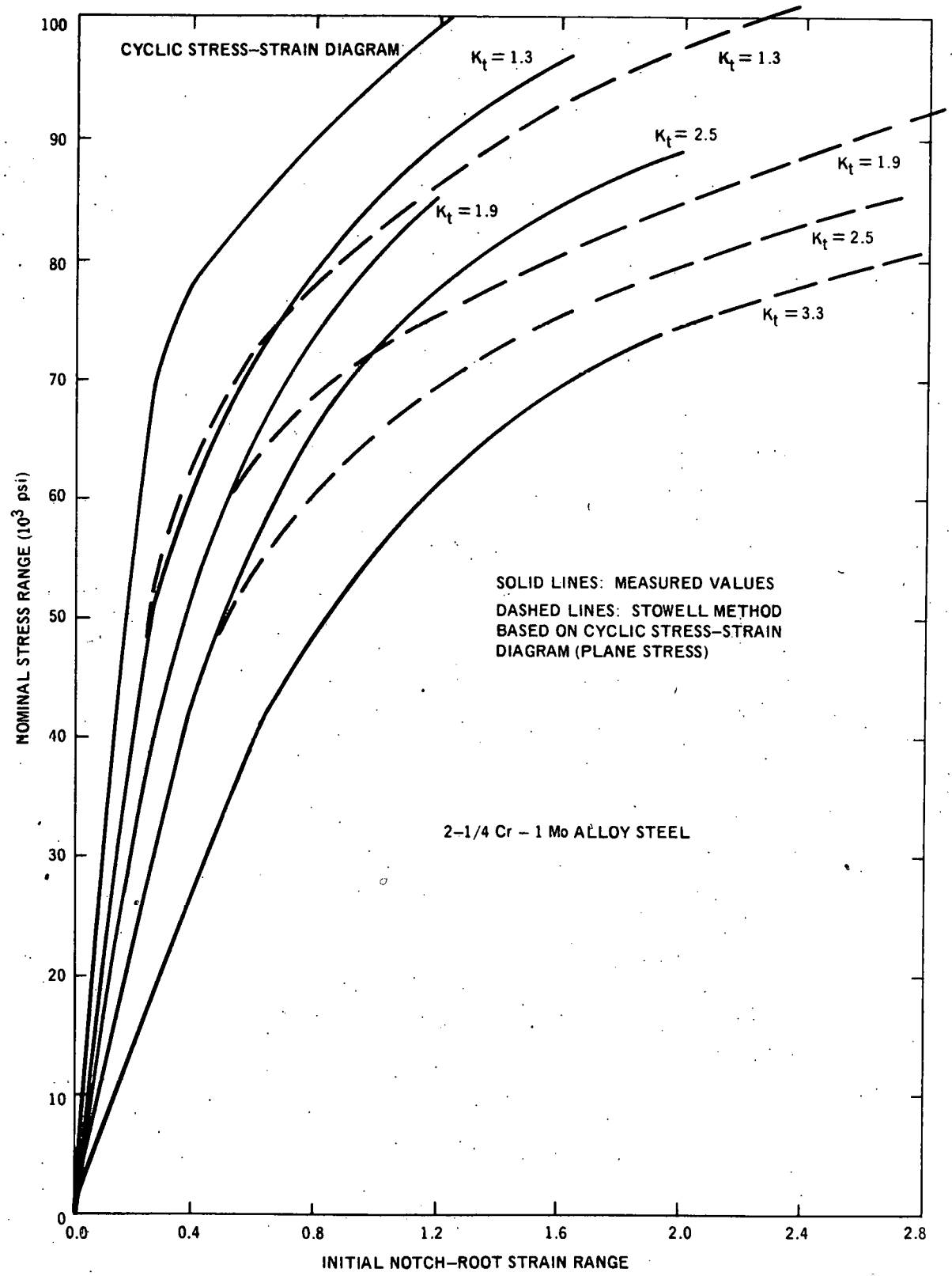

Figure 21. Comparison of Calculated and Measured Nominal Stress Range - Notch-Root Strain Range Diagrams. Material: 2-1/4 Cr–1 Mo Alloy Steel. Room Temperature.

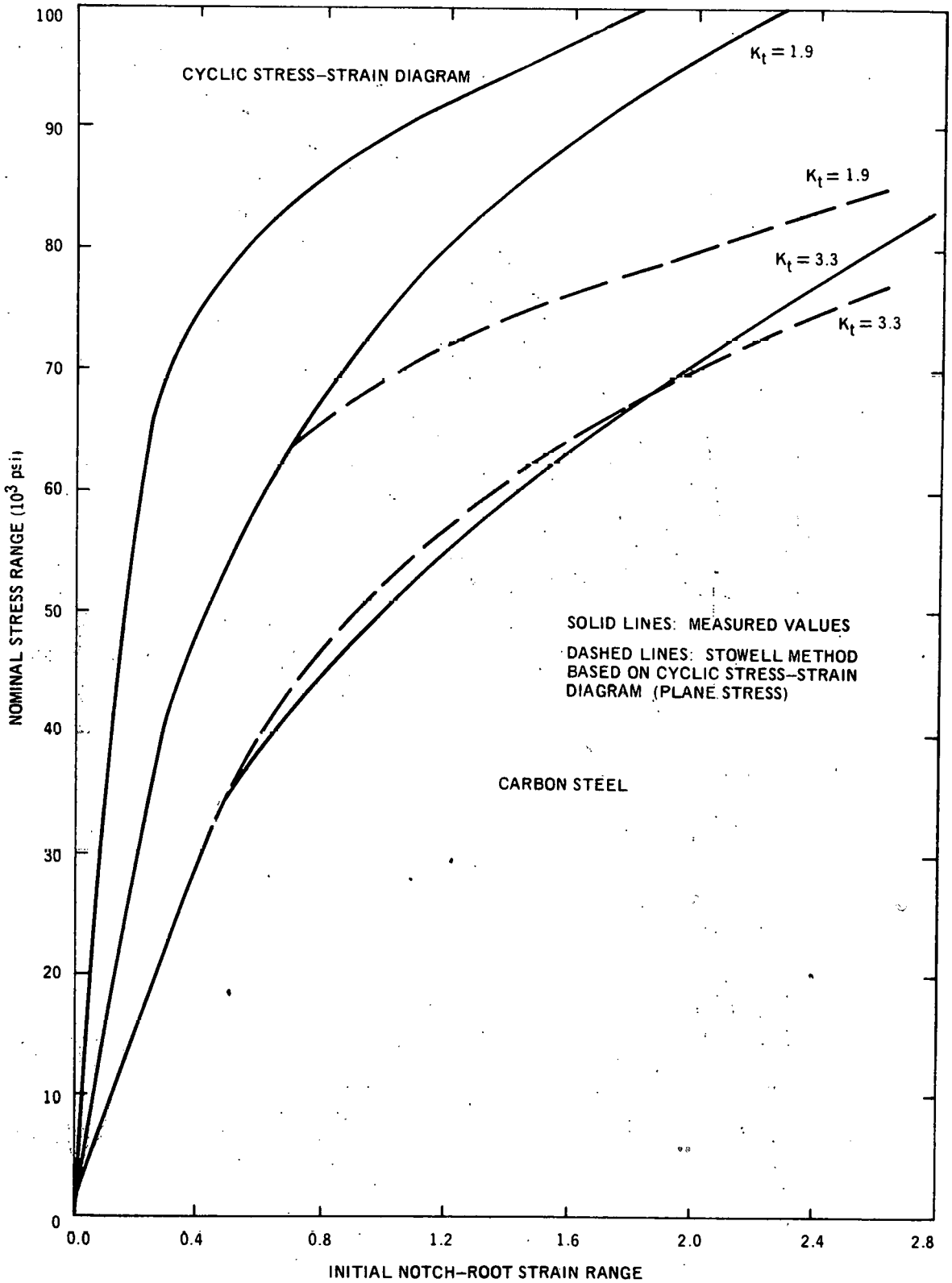

Figure 22. Comparison of Calculated and Measured Nominal Stress Range - Notch-Root Strain Range Diagrams. Material: Carbon Steel. Room Temperature.

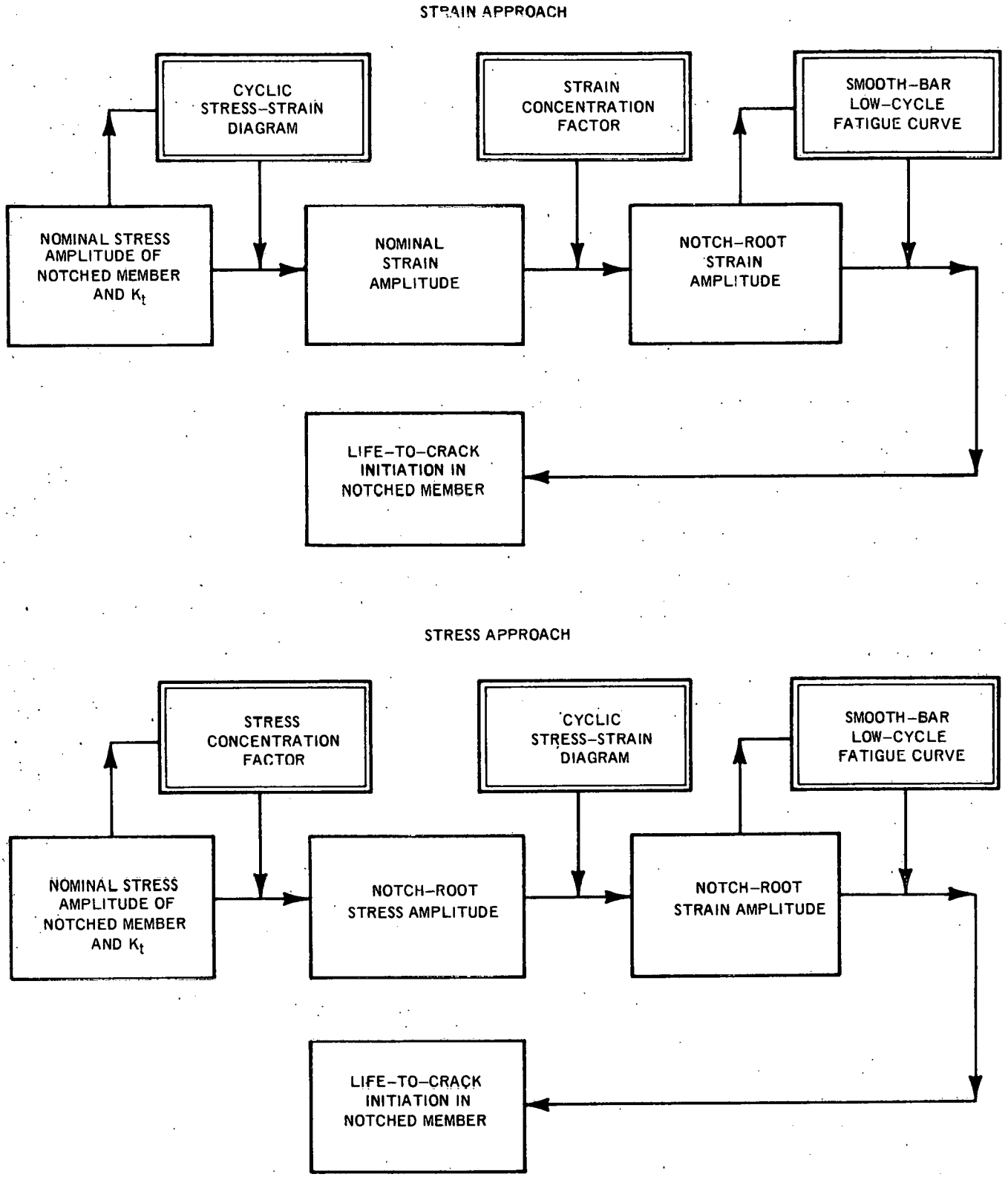

Figure 23. Schematic Illustrating Stress and Strain Approach for the Calculation of Notch-Root Strain Range and Fatigue Life-To-Crack Initiation. Boxes Enclosed by Double Lines Designate Information Which Must Be Obtained from Smooth-Bar Data.

ACKNOWLEDGMENT

The author is indebted to many individuals of the General Electric Materials and Processes Laboratory, Schenectady, New York who helped to complete this experimental task. Special acknowledgment is due to Messrs. R. J. Schaaff and R. H. Urich. Dr. S. Yukawa provided expert management and many helpful discussions, as well as editorial assistance. His contributions are gratefully acknowledged.

REFERENCES

1. Krempl, E., *Influence of Stress-Strain Concentration and Mean Stress on the Low-Cycle Fatigue Behavior of Three Structural Steels at Room Temperature*, GEAP-5726, September 1968.
2. *Reactor Primary Coolant Rupture Study—Quarterly Progress Report No. 10*, GEAP-5554, 1967.
3. Krempl, E., *The 550°F Notched High-Strain Fatigue Behavior of Three Low-Strength Structural Steels*, GEAP-10090, August 1969.
4. *Reactor Primary Coolant Rupture Study—Quarterly Progress Report No. 12*, GEAP-5680, 1968.
5. Tagart, S. W., "Plastic Fatigue Analysis of Pressure Components," *ASME Paper 68-PVP-3*, 1968.
6. Krempl, E., *Notched High-Strain Fatigue Behavior of Three Low-Strength Structural Steels*, Proceedings First International Conference on Pressure Vessel Technology, II, ASME, 1969.
7. Stowell, E. Z., "Stress and Strain Concentration at a Circular Hole in an Infinite Plate," *NACA, TN-2073* 1950.
8. Neuber, H., "Theory of Stress Concentration for Shear-Strained Prismatical Bodies with Arbitrary Nonlinear Stress-Strain Law," *Trans. ASME*, **83**, Series E, pp. 544-550, (1961).
9. Krempl, E., "Cyclic Plasticity—Some Properties of the Hysteresis Curve of Structural Metals at Room Temperature," *ASME Paper WA-69/MET-4*, 1969.
10. Topper, T. H., Wetzel, R. M., and Morrow, J. D., "Neuber's Rule Applied to Fatigue of Notched Specimens," *Journal of Materials*, **4**, No. 1, 1969, pp 200-209.

DISTRIBUTION

Aerojet General
Engineering Division
Sacramento Plant
Sacramento, California 95801
Attn. Dr. F.J. Climent — 1

Advisory Committee on Reactor Safeguards
Dr. Spencer H. Bush
Consultant to the Director
Battelle Memorial Institute
Pacific Northwest Laboratory
Richland, Washington 99352 — 1

Advisory Committee on Reactor Safeguards
Mr. Harold Etherington
84 Lighthouse Drive
Jupiter, Florida 33458 — 1

Advisory Committee on Reactor Safeguards
Dr. William L. Faith
2540 Huntington Drive
San Marino, California 91108 — 1

Advisory Committee on Reactor Safeguards
Dr. Chester P. Siess
Department of Civil Engineering
3129 Civil Engineering Bldg.
University of Illinois
Urbana, Illinois 61801 — 1

Advisory Committee on Reactor Safeguards
Dr. Stephen H. Hanauer
Professor of Nuclear Engineering
606 Dougherty Hall
University of Tennessee
Knoxville, Tennessee 37916 — 1

Advisory Committee on Reactor Safeguards
Dr. Joseph M. Hendrie
Nuclear Engineering Department
Brookhaven National Laboratory
Upton, New York 11973 — 1

Advisory Committee on Reactor Safeguards
Dr. Herbert S. Isbin
Department of Chemical Engineering
University of Minnesota
Minneapolis, Minnesota 55455 — 1

Advisory Committee on Reactor Safeguards
Mr. Harold G. Mangelsdorf
78 Knollwood Road
Short Hills, New Jersey 07078 — 1

Advisory Committee on Reactor Safeguards
Dr. Harry O. Monson, Senior Engineer
Laboratory Director's Office
Argonne National Laboratory
9700 South Cass Avenue
Argonne, Illinois 60439 — 1

Atomic Energy Commission
Division of Reactor Development and Technology
Washington, D.C. 20545
Attn: Mr. S.A. Szawlewicz — 5

Atomic Energy Commission
Division of Reactor Development and Technology
Washington, D.C. 20545
Attn: Mr. R.R. Newton — 1

Atomic Energy Commission
Division of Production
Washington, D.C. 20545
Attn: Mr. George B. Pleat — 1

Atomic Energy Commission
c/o Gulf General Atomic, Inc.
P.O. Box 608
San Diego, California 92112
Attn: Mr. Russell H. Ball — 1

Atomics International
P.O. Box 309
Canoga Park, California
Attn: Dr. H. Morewitz — 2

Babcock & Wilcox Company
Washington Operations Office
1725 I Street, N.W.
Washington,D.C. 20006 — 1

Babcock & Wilcox Company
P.O. Box 1260
Lynchburg, Virginia
Attn: Mr. Robert Wascher — 1

Battelle Memorial Institute
505 King Avenue
Columbus, Ohio 43201
Attn: Dr. D.N. Sunderman — 2

Battelle Memorial Institute
505 King Avenue
Columbus, Ohio 43201
Attn: Dr. D.L. Morrison — 1

Battelle Memorial Institute
505 King Avenue
Columbus, Ohio 43201
Attn: Mr. S. Paprocki — 2

Battelle Memorial Institute
505 King Avenue
Columbus, Ohio 43201
Attn: Mr. A.R. Duffy — 1

Brookhaven National Laboratory
Upton, Long Island, New York 11973
Attn: A.W. Castleman — 1

Advisory Committee on Reactor Safeguards 1
Dr. Arlie A. O'Kelly
2421 West Rowland Avenue
Littleton, Colorado 80120

Advisory Committee on Reactor Safeguards 1
Dr. David Okrent, Senior Physicist
Laboratory Director's Office
Argonne National Laboratory
9700 South Cass Avenue
Argonne, Illinois 60439

Advisory Committee on Reactor Safeguards 1
Dean Nunzio J. Palladino
College of Engineering
The Pennsylvania State University
101 Hammond Building
University Park, Pennsylvania 16802

Advisory Committee on Reactor Safeguards 1
Dr. William R. Stratton
Los Alamos Scientific Laboratory
P. O. Box 1663
Los Alamos, New Mexico 87544

Advisory Committee on Reactor Safeguards 1
Dr. Carroll W. Zabel
Director of Research
University of Houston
Cullen Boulevard
Houston, Texas 77004

Mr. Raymond F. Fraley 3
Executive Secretary
Advisory Committee on Reactor Safeguards
U.S. Atomic Energy Commission
Room 1034-H
Washington, D.C. 20545

Argonne National Laboratory 1
9700 South Cass Avenue
Argonne, Illinois
Attn: Mr. Paul G. Shewmon

Argonne National Laboratory 1
9700 South Cass Avenue
Argonne, Illinois
Attn: Dr. P. Lottes

Argonne National Laboratory 1
9700 South Cass Avenue
Argonne, Illinois
Attn: Dr. C.E. Dickerman

Argonne National Laboratory 1
9700 South Cass Avenue
Argonne, Illinois
Attn: Dr. R.O. Ivins

Argonne National Laboratory 1
9700 South Cass Avenue
Argonne, Illinois
Attn: Dr. S. Fistedis

Argonne National Laboratory 1
9700 South Cass Avenue
Argonne, Illinois
Attn: Dr. R.C. Vogel

Argonne National Laboratory 1
9700 South Cass Avenue
Argonne, Illinois
Attn: LMFBR Program Office

Argonne National Laboratory 2
9700 South Cass Avenue
Argonne, Illinois
Attn: Mr. A. Amorosi

Argonne National Laboratory 1
9700 South Cass Avenue
Argonne, Illinois
Attn: Dr. L. Baker

Atomic Energy Commission 1
Division of Reactor Development and Technology
Washington, D.C. 20545
Attn: Col. R.L. Ednie
Asst. Director for Army Reactors

Atomic Energy Commission 1
Division of Reactor Development and Technology
Washington, D.C. 20545
Attn: Mr. M.A. Rosen
Asst. Director for Plant Engineering

Atomic Energy Commission 1
Division of Reactor Development and Technology
Washington, D.C. 20545
Attn: Mr. M.J. Whitman
Asst. Director for Program Analysis

Atomic Energy Commission 1
Division of Reactor Development and Technology
Washington, D.C. 20545
Attn: Dr. E.E. Sinclair
Asst. Director for Reactor Technology

Atomic Energy Commission 1
Division of Reactor Development and Technology
Washington, D.C. 20545
Attn: Mr. A. Giambusso
Asst. Director for Project Management

Atomic Energy Commission 1
Division of Reactor Development and Technology
Washington, D.C. 20545
Attn: Mr. E.E. Kintner
Asst. Director for Reactor Engineering

Atomic Energy Commission 1
Division of Reactor Development and Technology
Washington, D.C. 20545
Attn: Mr. J. W. Crawford
Asst. Director for Engineering Standards

Atomic Energy Commission
Division of Compliance, Region IV
10395 West Colfax Avenue
Denver, Colorado 80215
Attn: Mr. John W. Flora — 1

Atomic Energy Commission
Division of Compliance
Washington, D.C. 20545
Attn: Mr. L. Kornblith, Jr. — 1

Atomic Energy Commission
Division of Operational Safety
Washington, D.C. 20545
Attn: Mr. H. Gilbert — 1

Atomic Energy Commission
Division of Reactor Standards
Washington, D.C. 20545
Attn: Mr. E.G. Case — 10

Atomic Energy Commission
Division of Reactor Standards
Washington, D.C. 20545
Attn: Mr. M. Bolotsky — 1

Atomic Energy Commission
Division of Reactor Standards
Washington, D.C. 20545
Attn: Mr. A.B. Holt — 1

Atomic Energy Commission
Division of Reactor Standards
Washington, D.C. 20545
Attn: Mr. R. Waterfield — 1

Atomic Energy Commission
Division of Reactor Standards
Washington, D.C. 20545
Attn: Dr. G. Burley — 1

Atomic Energy Commission
Division of Reactor Standards
Washington, D.C. 20545
Attn: Mr. R. Impara — 1

Atomic Energy Commission
Water Projects Branch
Division of Reactor Development and Technology
Washington, D.C. 20545
Attn: Mr. W.H. Layman — 1

Atomic Energy Commission
Naval Reactors Branch
Division of Reactor Development and Technology
Washington, D.C. 20545
Attn: Mr. R.S. Brodsky — 2

Atomic Energy Commission
Division of Reactor Development and Technology
Washington, D.C. 20545
Attn: A.J. Pressesky — 7

University of California
Institute of Engineering Research
Berkeley, California 94704
Attn: Prof. V.E. Schrock — 1

University of California
Institute of Engineering Research
Berkeley, California 94704
Attn: Prof. H.A. Johnson — 1

Canoga Park Area Office
P.O. Box 591
Canoga Park, California 91305
Attn: Mr. R.L. Morgan RDT Senior Site Rep. — 1

Combustion Engineering, Inc.
Nuclear Division
P.O. Box 500
Windsor, Connecticut 06095
Attn: Mr. M.F. Valerino — 1

Chicago Operations Office
Atomic Energy Commission
9800 South Cass Avenue
Argonne, Illinois 60439
Attn: Mr. D.M. Gardiner — 1

Douglas United Nuclear
Richland, Washington
Attn: Mr. John Riches — 1

Harvard Air Cleaning Laboratory
Harvard University
665 Huntington Avenue
Boston, Massachusetts 02190 — 1

IIT Research Institute
10 W. 35th Street
Chicago, Illinois 60616
Attn: Dr. T.A. Zaker — 1

IIT Research Institute
10 W. 35th Street
Chicago, Illinois 60616
Attn: Mr. E.V. Gallagher — 1

Idaho Operations Office
Atomic Energy Commission
P.O. Box 2108
Idaho Falls, Idaho 83401
Attn: Mr. D. Williams — 2

Liquid Metal Engineering Center
c/o Atomics International
P.O. Box 309
Canoga Park, California 91304
Attn: R.W. Dickinson — 1

Los Alamos Scientific Laboratory
P.O. Box 1663
Los Alamos, New Mexico 87544
Attn: Mr. J.H. Russel, K Division — 1

MPR Associates, Inc. 1
1140 Connecticut Avenue, N.W.
Washington, D.C. 20036
Attn: Mr. T. Rockwell III
Chairman AIF Safety Task Force

National Bureau of Standards 1
Washington, D.C. 20545
Attn: Dr. C. Muehlhause

Naval Ordnance Laboratory 1
White Oak
Silver Spring, Maryland
Attn: Mr. James Proctor

North Carolina State University 1
Department of Mechanical Engineering
Raleigh, North Carolina 27607
Attn: Prof. M.N. Ozisik

Nuclear Fuels Services 1
West Valley, New York 14171

Oak Ridge Operations Office 1
Atomic Energy Commission
Oak Ridge, Tennessee 37830
Attn: Mr. W.L. Smalley

Oak Ridge National Laboratory 1
Nuclear Safety Information Center
P.O. Box Y
Oak Ridge, Tennessee 37830
Attn: Mr. Joel Buchanan

Chemical Technology Division 1
Oak Ridge National Laboratory
P.O. Box Y
Oak Ridge, Tennessee 37830
Attn: Mr. D. Ferguson

Chemical Technology Division 1
Oak Ridge National Laboratory
P.O. Box Y
Oak Ridge, Tennessee 37830
Attn: Mr. R. Blanco

Oak Ridge National Laboratory 2
P.O. Box Y
Oak Ridge, Tennessee
Attn: HTGR Safety Program Office

Oak Ridge National Laboratory 4
P.O. Box Y
Oak Ridge, Tennessee
Attn: Mr. W. B. Cottrell

Oak Ridge National Laboratory 1
P.O. Box Y
Oak Ridge, Tennessee
Attn: Mr. P. Rittenhouse

Pacific Northwest Laboratories 1
P.O. Box 999
Richland, Washington 99352
Attn: Mr. G. Rogers

Pacific Northwest Laboratories 1
P.O. Box 999
Richland, Washington 99352
Attn: Mr. J.C. Spanner

Pacific Northwest Laboratories 1
P.O. Box 999
Richland, Washington 99352
Attn: Dr. J. Batch

Pacific Northwest Laboratories 2
P.O. Box 999
Richland, Washington 99352
Attn: Mr. R. Nightingale

Pacific Northwest Laboratories 1
P.O. Box 999
Richland, Washington 99352
Attn: Mr. L. Schwendiman

Pacific Northwest Laboratories 1
P.O. Box 999
Richland, Washington 99352
Attn: Mr. E.R. Astley, Mgr. FFTF

Idaho Nuclear Corporation 1
P.O. Box 1845
Idaho Falls, Idaho 83401
Attn: Mr. Curt Haire

Idaho Nuclear Corporation 2
P. O. Box 1845
Idaho Falls, Idaho 83401
Attn: Mr. S. O. Johnson

Idaho Nuclear Corporation 2
P.O. Box 1845
Idaho Falls, Idaho 83401
Attn: Mr. H. L. Coplen

Idaho Nuclear Corporation 1
P. O. Box 1845
Idaho Falls, Idaho 83401
Attn: Mr. O. F. Brockett

Idaho Nuclear Corporation 3
P. O. Box 1845
Idaho Falls. Idaho 83401
Attn: Water Reactor Safety Program
Office, Mr. G. O. Bright, Mgr.

Richland Operations Office 1
P.O. Box 500
Richland, Washington 99352
Attn: Mr. C. Robinson

Richland Operations Office 1
P.O. Box 500
Richland, Washington 99352
Attn: Mr. A.S. Waterhouse

Richland Operations Office 1
P.O. Box 500
Richland, Washington 99352
Attn: Mr. A. Brunstad

Dr. P. L. Pfenningwerth
Bettis Atomic Power Laboratory
P.O. Box 79
West Mifflin, Pennsylvania 15122 — 1

Professor C.E. Taylor
Department of Theoretical and Applied Mechanics
University of Illinois
Urbana, Illinois — 1

Mr. E. Beauchamp-Nobbs
U.S. Marine Engineering Laboratory
Annapolis, Maryland — 1

U.S. Atomic Energy Commission
Division of Technical Information Extension
P.O. Box 62
Oak Ridge, Tennessee — 3

U.S. Atomic Energy Commission
Division of Reactor Licensing
Washington, D.C. 20545
Attn: S.S. Pawlicki — 1

USAEC Site Representative
General Electric Company
Sunnyvale, California 94086
Attn: Joel Levy, Senior Site Rep. — 1

Mr. B.L. Greenstreet
P.O. Box Y
Oak Ridge National Laboratory
Oak Ridge, Tennessee — 1

Mr. F.J. Witt
P.O. Box Y
ORNL - Oak Ridge, Tennessee — 1

Commonwealth Edison Company
Dresden Nuclear Power Station
Rural Route 1
Morris, Illinois 60450
Attn: H.K. Hoyt — 2

Commonwealth Edison Company
System Mechanical and Structural Engineer
72 West Adams Street
Chicago, Illinois 60690
Attn: N.A. Kershaw — 3

United Kingdom Atomic Energy Authority
Reactor Materials Laboratory
Wigshaw Lane, Culcheth
Warrington, Lancs.
England
Attn: R.W. Nichols — 1

Atomic Energy of Canada Limited
Chalk River Nuclear Laboratories
Chalk River, Ontario, Canada
Dr. George Pon — 1

San Francisco Operations Office
Atomic Energy Commission
2111 Bancroft Way
Berkeley, California 94704
Attn: Mr. C.V. Backlund — 1

Savannah River Laboratories
E.I. duPont deNemours and Company
Aiken, South Carolina 29802
Attn: Mr. A.H. Peters — 1

TRW Inc.
TRW Systems Group
One Space Park
Redondo Beach, California 90278
Attn: Dr. D. B. Langmuir — 1

TRW Inc.
TRW Systems Group
One Space Park
Redondo Beach, California 90278
Attn: Mr. S.M. Zivi — 1

Westinghouse Electric Corporation
Atomic Power Division
P.O. Box 355
Pittsburgh, Pennsylvania 15230
Attn: Mr. R.A. Wiesemann — 1

Westinghouse Electric Corporation
Atomic Power Division
P.O. Box 355
Pittsburgh, Pennsylvania 15230
Attn: Dr. D. Fletcher — 1

Westinghouse Electric Corporation
Atomic Power Division
P.O. Box 355
Pittsburgh, Pennsylvania 15230
Attn: Dr. E. Beckjord — 1

Westinghouse Electric Corporation
P.O. Box 19218
Tampa, Florida 33616
Attn: Mr. A. Lohmeier — 1

Southern Nuclear Engineering, Inc.
P.O. Box 10
Dunedin, Florida 33528
Attn: Mr. Gilbert Brown — 1

Holmes & Narver, Inc.
828 South Figueroa St.
Los Angeles, California 90017
Attn: B. Shimizu — 1

Mr. Edward T. Wessel
Research and Development Center
Westinghouse Electric Corporation
Beulah Road, Churchill Boro
Pittsburgh, Pennsylvania 15235 — 1

O.A. Kellerman
Institut Fur Reaktorsicherheit
Der Technischen Uberwachungs
Vereine, e.V.
5 Koln - Ehrenfeld, Lukasstr. 90
West Germany — 1

C. A. G. Phillips
U.K.A.E.A. Safeguards Division
Authority Health & Safety Branch
Risley, Warrington, Lancashire
England — 1

Knolls Atomic Power Laboratory
P. O. Box 1072
Schenectady, New York 12301
Attn: Dr. Robert A. Barnes — 1

Reactor Materials Branch
Metallurgy Division
Naval Research Laboratory
Washington, D. C. 20545
Attn: Mr. L. E. Steele — 1

Department of Material Science & Engineering
Hearst Mining Building
University of California
Berkeley, California
Attn: Mr. William W. Gerberich — 1

Argonne National Laboratory
9700 South Cass Avenue
Argonne, Illinois
Attn: Mr. Craig Cheng — 1

Division of Reactor Development & Technology
U.S. Atomic Energy Commission
Washington, D.C. 20545
Attn: J. R. Hunter — 1

United Engineers and Constructors, Inc.
1401 Arch Street
Philadelphia, Pennsylvania 19105
Attn: Mr. John Crowley — 1

Mr. Robert D. Wylie
Department of Materials Engineering
Southwest Research Institute
8599 Culebra Road
San Antonio, Texas 78228 — 1

AEG Telefunken
AEC Hochhaus Sued
6 Frankfurt/Main 70
West Germany
Attn: Mr. Dieter Ewers — 1

Dr. William E. Cooper
Teledyne Materials Research
303 Bear Hill Road
Waltham, Massachusetts — 1

Roger W. Staehle
Metallurgy Department
Ohio State University
Columbus, Ohio — 1

Mr. Ralph Jones
Division of Reactor Development
U.S. Atomic Energy Commission
Washington 25, D.C. — 1

Mr. H.K. Marks
Room 2N83
Department of the Navy
Washington, D.C. — 1

H. Thielsch
140 Shaw Avenue
Cranston 5, Rhode Island — 1

Mr. F.M. Moschine
Westinghouse Electric Company
Atomic Power Department
P.O. Box 355
Pittsburgh, Pennsylvania 15230 — 1